THE GEOLOGICAL SOCIETY OF AMERICA®

Geochronology and geochemistry of Neoproterozoic granitoids in the central Qilian Shan of northern Tibet: Reconstructing the amalgamation processes and tectonic history of Asia

Chen Wu[1,*], Andrew V. Zuza[2,3], An Yin[1,2], Changfeng Liu[4], Robin C. Reith[2], Jinyu Zhang[5], Wencan Liu[4], and Zhiguang Zhou[1]

[1]STRUCTURAL GEOLOGY GROUP, CHINA UNIVERSITY OF GEOSCIENCES (BEIJING), BEIJING 100083, CHINA
[2]DEPARTMENT OF EARTH, PLANETARY, AND SPACE SCIENCES, UNIVERSITY OF CALIFORNIA, LOS ANGELES, CALIFORNIA 90095-1567, USA
[3]NEVADA BUREAU OF MINES AND GEOLOGY, UNIVERSITY OF NEVADA, RENO, NEVADA 89557, USA
[4]INSTITUTE OF GEOLOGICAL SURVEY, CHINA UNIVERSITY OF GEOSCIENCES (BEIJING), BEIJING 100083, CHINA
[5]INSTITUTE OF GEOLOGY, CHINA EARTHQUAKE ADMINISTRATION, BEIJING 100029, CHINA

ABSTRACT

Our understanding of the assembly history of Asia depends critically on the tectonic relationships between its major cratons, including Siberia, North China, South China, and Tarim. The intervening microcontinents between these cratons can provide insight into the paleogeographic and paleotectonic relationships of the cratons, but there is currently a general lack of knowledge regarding the basement geology of these microcontinents. Here we present results from systematic geologic mapping, U-Pb zircon dating, whole-rock geochemical analysis, and synthesis of existing data to establish the Proterozoic to early Paleozoic evolution of the central Qilian basement to the south of the North China craton in northwest China. Our results indicate that the region underwent three major periods of magmatic activity at 960–880, 877–710, and 550–375 Ma. Our geochemical analysis suggests that the ca. 900 Ma plutons were generated during arc magmatism and/or syncollisional crustal melting, whereas the ca. 820 Ma plutons are A-type granitoids, which are typically associated with extensional tectonism. Igneous zircons from a high- and ultrahigh-pressure eclogite in the north-central Qilian Shan have a U-Pb age of ca. 916 Ma, whereas dating of the recrystallized rims suggests that eclogite facies metamorphism occurred at ca. 485 Ma. Our detrital zircon geochronology also indicates that a widespread metasedimentary unit in the region was deposited between ca. 1200 and ca. 960 Ma, prior to the onset of a rift-drift event at ca. 750 Ma. Based on regional geologic constraints and the magmatic history, we propose the following tectonic history: (1) the paleo–Qilian Ocean bound the combined North Tarim–North China craton to the south (present-day coordinates) in the Mesoproterozoic; (2) the paleo–Qilian Ocean closed between 900 and 820 Ma following the collision of North Tarim–North China craton and the South Tarim–Qaidam–Kunlun continent; (3) the younger Qilian Ocean opened at ca. 775 Ma along the previous suture trace of the paleo–Qilian Ocean as a marginal sea within southern Laurasia; and (4) this ocean closed by ca. 445–440 Ma as a result of collision between the Tarim–North China cratons and the Qaidam-Kunlun continent along a south-dipping subduction system.

LITHOSPHERE; v. 9; no. 4; p. 609–636; GSA Data Repository Item 2017231 | Published online 25 May 2017 https://doi.org/10.1130/L640.1

INTRODUCTION

Northern Tibet marks the transitional zone between the Tethyan orogenic system to the south and the Paleo–Asian Ocean system to the north (Fig. 1) (e.g., Şengör and Natal'in, 1996; Yin and Harrison, 2000; Heubeck, 2001; Stampfli and Borel, 2002; Stampfli et al., 2013; Wu et al., 2016). Although extensive research has focused on the tectonic evolution of these two well-known orogenic domains, comparatively little research has been devoted to investigating the tectonic history of intervening oceanic and continental fragments, including the early Paleozoic Qilian orogen (e.g., Yin et al., 2007a; Xiao et al., 2009; Song et al., 2013). A major challenge in unraveling the geologic history of the Qilian orogen is that the region was strongly modified by later phases of Mesozoic extension and Cenozoic intracontinental thrust and strike-slip faulting (Fig. 1) (Yin and Harrison, 2000; Chen et al., 2003; Cowgill et al., 2003; Yin, 2010; Gao et al., 2013; Zuza and Yin, 2016; Zuza et al., 2016).

Early workers suggested that the ophiolite-bearing mélange and blueschist assemblages exposed across the Qilian Shan represented an early Paleozoic Qilian Ocean (Wang and Liu, 1976; Xiao et al., 1978). Later studies revealed that the Qilian Ocean may have formed as early as the Neoproterozoic (e.g., Yin and Harrison, 2000; Gehrels et al., 2003a, 2003b, 2011; Yin et al., 2007a; Xiao et al., 2009; Song et al., 2013, 2014; Xu et al., 2015; Wu et al., 2016). However, the lack of absolute age constraints and an unclear geologic context of the Neoproterozoic strata have hampered our ability to decipher the origin and formation ages of this ocean. This has in turn led to debates regarding (1) the location and lateral extent of the Qilian Ocean as represented by the suture zone rocks (e.g., Tseng et al., 2009), (2) the polarity of subduction that led to the closure of the Qilian Ocean (e.g., Zuo and Liu, 1987; Feng and He, 1996; Yin and Harrison, 2000; Yang et al., 2002; C.L. Wu et al., 2006; Gehrels et al., 2003a, 2003b,

*Corresponding author: wuchenlovegeology@gmail.com; wuchen2016@cugb.edu.cn

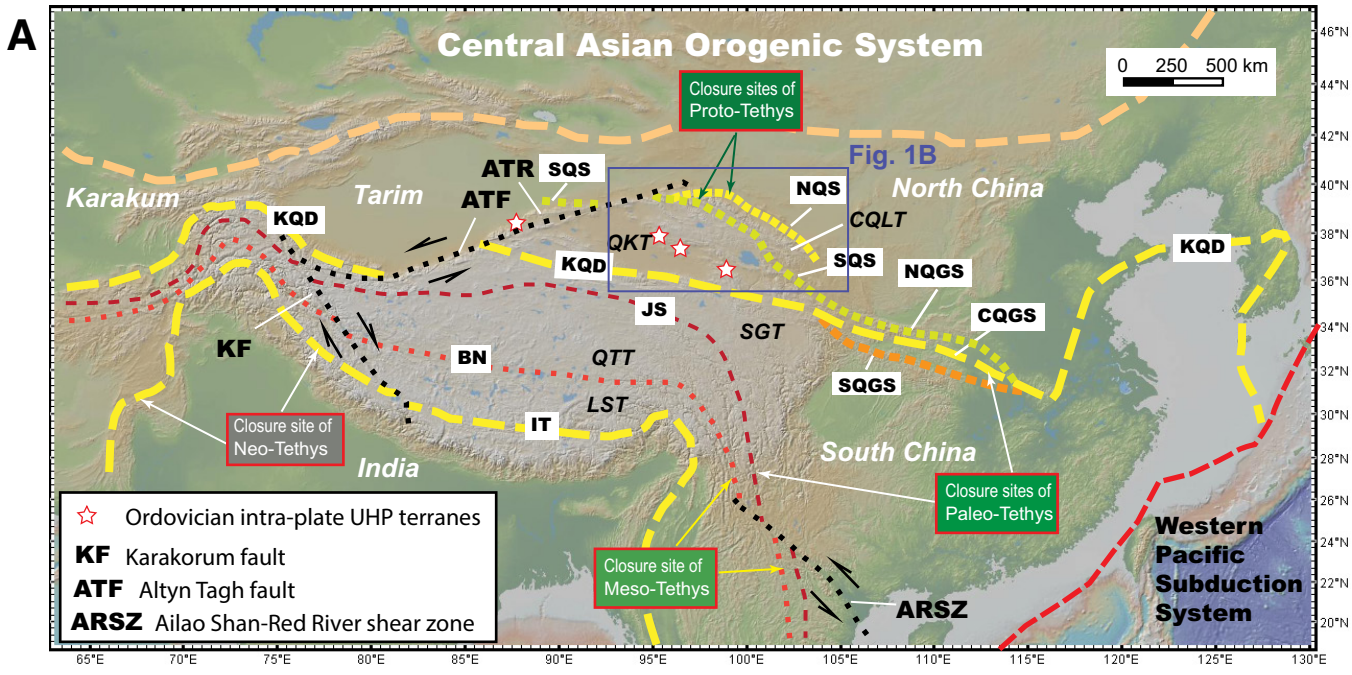

KQD: Kunlun-Qinling-Dabie suture; NQS and SQS: North and South Qilian sutures; NQGS, CQGS, and SQGS: North, Central, and South Qinling suture; JS: Jinsha suture; BN: Bangong-Nujiang suture; IT: Indus-Tsangpo suture. QKT: Qaidam-Kunlun terrane; SGT: Songpan-Ganzi terrane; QTT: Qiangtang terrane; LST: Lhasa terrane; CQLT: central Qilian terrane; KF: Karakorum fault; ARSZ: Ailao Shan-Red River shear zone; ATF: Altyn Tagh fault; ATR: Altyn Tagh Range.

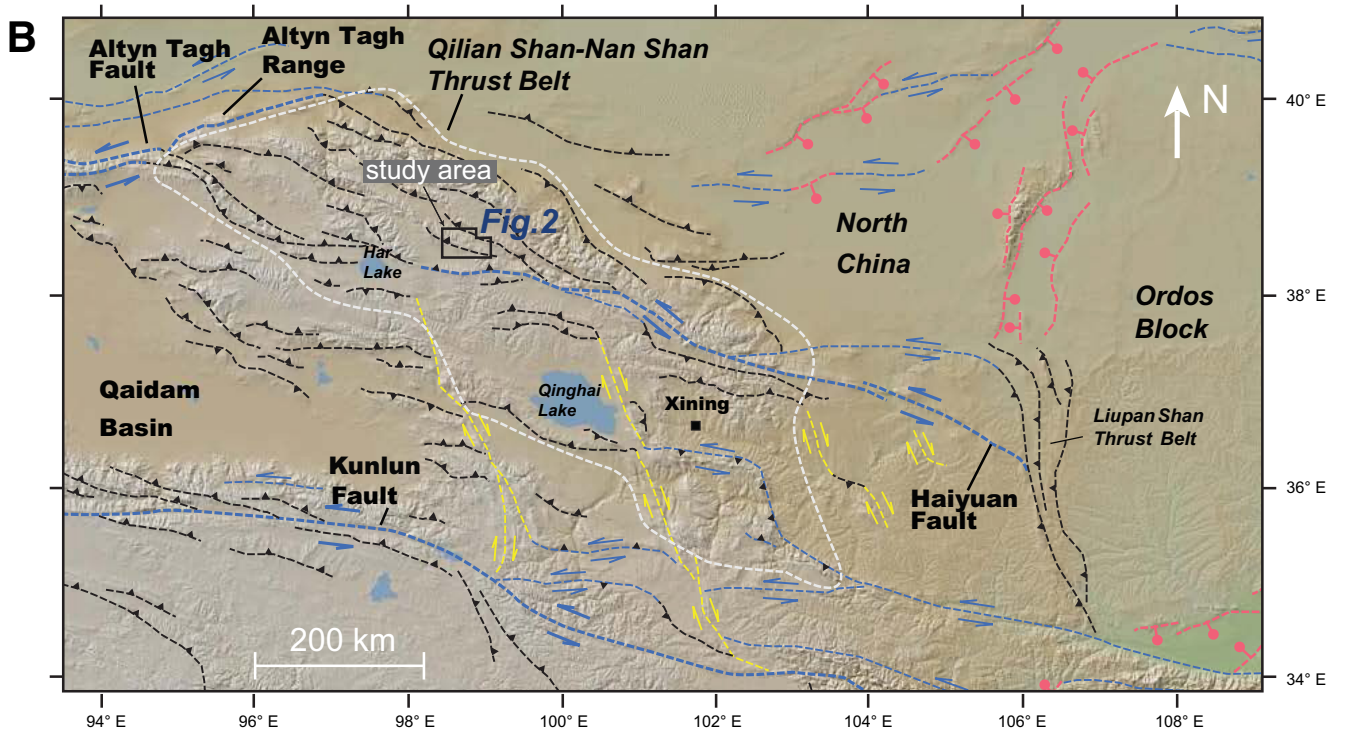

Figure 1. (A) Tectonic map of the Tethyan Orogenic System and the Central Asian Orogenic System (modified from Wu et al., 2016). (B) Regional tectonic map of the Qilian Shan–Nan Shan thrust belt and its adjacent regions (modified from Gao et al., 2013; Zuza et al., 2016). Major faults are denoted with black lines (thrust), blue lines (sinistral strike slip), yellow lines (dextral strike slip), and pink lines (normal). Underlying base map is from www.geomapapp.org (Ryan et al., 2009).

2011; Tung et al., 2007, 2013; Song et al., 2006, 2010, 2013, 2014; Huang et al., 2015; Xu et al., 2015), and (3) the lateral linkage of the Precambrian Qilian basement (Qaidam-Kunlun terrane), which is bounded by the north and south Qilian suture zones to the north and the Kunlun-Qinling-Dabie suture to the south (Fig. 1A), with either the North China or South China cratons (e.g., Zuo and Liu, 1987; Feng and He, 1996; Wan et al., 2001; Tung et al., 2007, 2013; Lu et al., 2008; Song et al., 2010, 2012, 2013; Xu et al., 2015; Wu et al., 2016) (Fig. 1). A Qilian–South China craton connection would require that the Qilian continental basement (Qaidam-Kunlun terrane) was first rifted from the Yangtze craton in the western part of the South China craton during the Neoproterozoic breakup of the supercontinent Rodinia and later collided against the North China craton in the early Paleozoic (e.g., Wan et al., 2001; Tung et al., 2007; Song et al., 2013; Xu et al., 2015). In contrast, a Qilian–North China connection requires that the Qaidam-Kunlun terrane never drifted far from the North China craton since the Neoproterozoic.

In this study we present new results based on detailed geologic mapping, U-Pb zircon geochronology, whole-rock geochemistry, and a synthesis of existing geological data across northern Tibet to determine the tectonic origin of the Proterozoic–early Paleozoic Qilian crystalline basement rocks. Our dating results suggest that magmatism occurred across the area at 960–880, 877–710, and 550–375 Ma, whereas our detrital zircon age analysis establishes links among key metasedimentary basement units. Integration of our new data with existing studies leads to a new reconstruction of the Proterozoic–Paleozoic development of northern Tibet that involves the closure of the Paleo–Qilian and Qilian Oceans in the Neoproterozoic and Late Ordovician, respectively.

REGIONAL GEOLOGY

South China

The Precambrian basement of the South China craton, which is composed of the Yangtze block to the northwest and the Cathaysia block to the southeast (Zhao and Cawood, 2012; Cawood et al., 2013; Xu et al., 2014), consists almost exclusively of Proterozoic lithologies with only minor Archean rocks exposed in the Kongling area. This is unlike the North China craton basement that is dominated by Archean and Paleoproterozoic rocks (e.g., Li et al., 1995; Zhao and Cawood, 2012; Zhao et al., 2012). The Yangtze block Archean–Paleoproterozoic crystalline basement (i.e., Kongling Complex) is surrounded by late Mesoproterozoic to early Neoproterozoic fold-thrust belts, which are unconformably overlain by weakly metamorphosed Neoproterozoic strata (e.g., Banxi Group) and unmetamorphosed Sinian cover (Wang and Mo, 1995). The Kongling Complex consists predominantly of Archean tonalite-trondhjemite-granodiorite (TTG) gneisses (ca. 3.3–2.9 Ga) and metasedimentary rocks, which are intruded by the Paleoproterozoic (ca. 1.85 Ga) Quanqitan granite in the north and early Neoproterozoic (820–750 Ma) Huangling intrusive suite in the south. Wang et al. (2012) presented U-Pb ages and Hf data for detrital zircons from the Neoproterozoic strata (e.g., Xiajiang, Danzhou and Banxi groups) in the Nanhua rift basin to show that these groups were deposited from 800 to 730 Ma.

The Cathaysia block is composed of predominantly Neoproterozoic metamorphic rocks with only minor Paleoproterozoic and Mesoproterozoic lithologies, which are exposed in the Chencai, Badu, Wuyishan, Nanling, Yunkai, and Hainan areas (Zhao and Cawood, 2012). Other areas of the block are covered by Phanerozoic igneous (especially Mesozoic granitoids) and sedimentary rocks (Shu et al., 1995; Shu and Charvet, 1996). Paleoproterozoic rocks consist of 1890–1830 Ma granitoids and 1850–1815 Ma supracrustal rocks, which were metamorphosed at 1.89–1.88 Ga and locally reworked at 250–230 Ma (Yu et al., 2009). Mesoproterozoic basement rocks (1431–1200 Ma) are restricted to Hainan Island (Li et al., 2002; X.H. Li et al., 2008a). A compilation of U-Pb zircon ages shows that >90% of the Cathaysia block Precambrian basement consists of Neoproterozoic rocks, including volcanic-sedimentary strata metamorphosed from greenschist to granulite facies (Zhao and Cawood, 2012). The Cathaysia block underwent a widespread tectonothermal event in the early Paleozoic, resulting in an angular unconformity between Devonian cover and metamorphosed pre-Silurian strata (Huang, 1977; Wang et al., 2013b).

In the recent reconstruction (Wu et al., 2016), the Yangtze basement is assumed to extend west underneath the Songpan-Ganzi terrane (see discussion in Zhang et al., 2014) and this entire craton rifted from Gondwana in the Devonian–Carboniferous (e.g., Zhao and Cawood, 2012; Cawood et al., 2013). The craton was bound to the north by the Neo–Kunlun Ocean (Mianlue Ocean) (e.g., Ratschbacher et al., 2003; Dong and Santosh, 2015) and the Jinsha Ocean to the south (e.g., Pullen et al., 2008; Ding et al., 2013), which are broadly equivalent to the suboceans of the Tethys Ocean (see Wu et al., 2016, for discussion), and collided with the North China craton along the Qinling-Dabie suture in the Permian–Triassic (Yin and Nie, 1993; Meng and Zhang, 1999; Ratschbacher et al., 2003; Hacker et al., 2004, 2006; Metcalfe, 2011; Dong and Santosh, 2015).

North China

The North China craton, also referred to as the Sino-Korean craton or platform, is bounded to the west-southwest by the early Paleozoic Qilian orogen and to the north by the Central Asian Orogenic System (Fig. 1A). The craton is traditionally divided into two major Archean–Proterozoic blocks separated by the Trans–North China orogen (e.g., Kröner et al., 2001, 2005, 2006; Kusky et al., 2007; Zhao and Cawood, 2012; Wan et al., 2015): (1) the Eastern block contains 3.8–2.6 Ga gneiss and greenstone belts overlain by 2.6–2.5 Ga metasedimentary cover; (2) the Western block consists of the Ordos and Yinshan blocks, which coalesced at ca. 1.92 Ga during the Khondalite orogen (e.g., Santosh et al., 2006, 2007; Zhao and Cawood, 2012). Paleoproterozoic rocks in the North China craton are generally related to the collisional assembly of the disparate parts of the Eastern and Western blocks, including a ca. 1.95 Ga collisional event that led to amalgamation of the Yinshan and Ordos blocks to form the Western block, which may have collided with the Eastern block during the ca. 1.85 Ga Trans–North China orogen (Zhao and Cawood, 2012). The timing and nature of the collision between the western and eastern North China craton is rigorously debated (e.g., Zhao et al., 1998, 1999, 2012; Li et al., 2000a, 2000b; Kusky and Li, 2003; Polat et al., 2005; Kröner et al., 2006; Li and Kusky, 2007; Faure et al., 2007; Trap et al., 2007, 2008, 2011, 2012; Kusky and Santosh, 2009; Xiao et al., 2011; Zhao and Cawood, 2012), and further discussion is not within the scope of this study.

In the late Mesoproterozoic, the northern margin of the NCC underwent rifting (i.e., the Bayan Obo rift zone) coincident with breakup of the Columbia supercontinent (Zhao and Cawood, 2012; Wan et al., 2015). The continuous Mesoproterozoic–Neoproterozoic sedimentation is observed in the Jixian county region of northern China. The strata can be divided into distinct successions: the Changcheng (1.8–1.6 Ga), Jixian (1.6–1.4 Ga), currently unnamed (1.4–1.0 Ga), and Qingbaikou (1.0–0.8 Ga) Groups (Wan et al., 2011; Sun et al., 2012). There are no middle to late Neoproterozoic (850–550 Ma) deposits in the Jixian region of northern China, and only minor sections in the Hu-Huai and Lushan-Ruyang regions (Zhang et al., 2006) to the south and the Liaodong Peninsula (Zhao and Cawood, 2012) to the east have reported strata of this age. Early Cambrian rocks unconformably overlie the uppermost section of Qingbaikou Group (i.e., the Jing'eryu Formation) rocks in the Jixian region (Sun et al., 2012).

Tarim

The Precambrian geology of the Tarim craton is inferred from drillcore and bedrock outcrops along the margins of the Tarim Basin (Fig. 1). Drillhole and geochronological observations support a ca. 1.0 Ga or earlier distinction between North and South Tarim, divided by a roughly northwest-trending suture zone through the middle of the present-day Tarim Basin (Guo et al., 2005; Xu et al., 2013; Zuza and Yin, 2014; Wu et al., 2016). Zircon ages from the Archean metamorphic rocks throughout Tarim (i.e., orthogneiss, TTG gneiss, and amphibolite enclaves) indicate a long-lived period of crustal growth at ca. 2.8–2.55 Ga (Mei et al., 1998; Lu et al., 2006). The oldest ages are from the Altyn Tagh Range (Fig. 1), where xenocrystic zircons have U-Pb ages of ca. 3.6 Ga (Lu et al., 2008). Paleoproterozoic metapelites unconformably overlie Archean basement (Gao et al., 1993), and early Paleoproterozoic magmatism occurred throughout Tarim, with observed ages ranging from 2.45 to 2.35 Ga (Lu, 2002; Lu et al., 2006, 2008). Granitoids with zircon ages of ca. 1.94–1.93 Ga intrude the Quruqtagh region (North Tarim) (Ge et al., 2015), and subsequently North Tarim underwent amphibolite to granulite facies metamorphism at 1.92–1.91 Ga (Lu et al., 2006, 2008; Ge et al., 2015). The presence of ca. 1.85 Ga and ca. 1.77 Ga mafic dikes in the Quruqtagh region (Xiao et al., 2003; Lu et al., 2006, 2008) may suggest an extensional setting during that time (Lu et al., 2006).

The Mesoproterozoic Ailiankate Group of South Tarim is inferred to represent an accreted island arc (Guo et al., 2004), whereas North Tarim is inferred to have been an undisturbed passive margin throughout most of the Mesoproterozoic (Wang et al., 2004). North and South Tarim may have collided at 0.9–0.8 Ga (Guo et al., 2005; Zuza and Yin, 2014) as evidenced by the pre–800 Ma Aksu blueshist (Nakajima et al., 1990; Chen et al., 2004), ca. 0.85 Ga argon cooling ages (Chen et al., 2004), and 830–800 Ma metamorphic zircon ages (Ge et al., 2016). The numerous 970–910 Ma granitoids reported throughout the Altyn Tagh Range (Cowgill et al., 2003; Gehrels et al., 2003a), Qilian Shan (Gehrels et al., 2003a; Tung et al., 2007, 2013; Wu et al., 2016; Zuza, 2016; this study), and Tian Shan (He et al., 2014) were possibly generated in the subduction system that accommodated the convergence between North and South Tarim and other adjacent continents (e.g., Wu et al., 2016).

The combined Tarim continent underwent bimodal volcanism and protracted rifting from ca. 870 Ma to ca. 630 Ma. In North Tarim, two or three distinct pulses of rift-related magmatic and/or plume activity occurred at 830–800 Ma, 790–740 Ma, and 650–630 Ma (e.g., Lu et al., 2008; Zhu et al., 2008; Shu et al., 2011). In South Tarim, bimodal volcanism and rift-basin development started as early as 900–870 Ma (Wang et al., 2015a, 2015b), which indicates that rifting along the Tarim southern margin initiated earlier than in the north. Rifting along Tarim's northern and southern margins is associated with the opening of the Paleo–Asian and Tethyan Oceans, respectively (e.g., Wu et al., 2016). Subsequently, the region was overlain by thick successions of latest Neoproterozoic to Cambrian passive continental margin deposits (Turner, 2010; Shu et al., 2011). The northern margin remained a passive continental shelf throughout much the Paleozoic (Graham et al., 1993). Late Paleozoic–Mesozoic arc magmatism observed along the southern margin of Tarim in the Western Kunlun Range (Cowgill et al., 2003) is related to northward subduction of the Neo–Kunlun Ocean (Paleo–Tethys Ocean) and arc development (Jiang et al., 1992; Cowgill et al., 2003; Wu et al., 2016).

Qilian Orogen

The early Paleozoic Qilian orogen is bound by the North China craton to north and the Qaidam-Kunlun terrane to the south (Şengör and Natal'in, 1996; Heubeck, 2001; Yin and Harrison, 2000; Song et al., 2013; Zuza et al., 2013, 2016; Wu et al., 2016). The orogen resulted from the closure of the Qilian Ocean during the collision between the Qaidam-Kunlun terrane and North China craton (e.g., Yin and Nie, 1996; Şengör and Natal'in, 1996; Sobel and Arnaud, 1999; Yin and Harrison, 2000; Gehrels et al., 2003a, 2003b; Yin et al., 2007a; Xiao et al., 2009; Song et al., 2013). It exposes Proterozoic to early Paleozoic crystalline and metasedimentary rocks with variable lithologies, and consists of two fragmented ophiolitic belts, commonly referred to as the North and South Qilian suture zones (Fig. 1). The North China craton is represented by Paleoproterozoic basement rocks and Mesoproterozoic cover sequences exposed throughout the Qilian Shan, possibly as orogen-scale windows, and in the Longshoushan region (Tung et al., 2007; Wan et al., 2013; Gong et al., 2013). The central Qilian basement, which is herein discussed as part of the Qaidam-Kunlun terrane (or microcontinent), consists of ca. 2.3 Ga basement rocks that may be correlated with North China (Dan et al., 2012). In the western Qilian Shan Proterozoic passive-margin strata were intruded by 900–960 Ma plutons (Gehrels et al., 2003a, 2003b) and were thrust below an eclogite-bearing metamorphic complex (Tseng et al., 2006). This metamorphic complex consists of 775–930 Ma orthogneiss (Tseng et al., 2006; Tung et al., 2007) and paragneiss with >880 Ma detrital zircon ages (Tung et al., 2007). In the east, Archean to Paleoproterozoic crystalline rocks are intruded by 750–1190 Ma plutons that are overlain by Neoproterozoic–Cambrian cratonal strata below and early Paleozoic arc assemblages (Guo et al., 1999; Wan et al., 2001; Tung et al., 2007).

The central Qilian basement consists of three Precambrian units: the Tuolai Group, Zhulongguan Group, and Tuolai Nanshan Group, from older to younger. The Tuolai Group is composed of gneiss, metabasite, schist, marble, and minor volumes of Proterozoic granitoids (Gansu Geological Bureau, 1989; Qinghai, 1991). The metasedimentary portion of the unit yielded ca. 1.8 Ga detrital zircon ages (Tung et al., 2007), and has been variably assigned to have been deposited in a passive-margin setting (Tung et al., 2007) or an arc setting (Wan et al., 2001; Smith, 2006). Zuza (2016) reported that the three youngest zircon grains of a biotite-plagioclase paragneiss from Tuolai Group with overlapping ages have a weighted mean age of ca. 1.5 Ga, which places its depositional age in the Mesoproterozoic. The Zhulongguan Group, which is interpreted to overlie the Tuolai Group, consists mainly of stromatolite-bearing limestone, basalt, and andesite. However, its contact with the presumably older Tuolai Group is not exposed (e.g., Pan et al., 2004; Xu et al., 2015). The youngest basement unit is the Tuolai Nanshan Group and its equivalent Gaolan and Huangyuan Groups, which consist of 930–775 Ma orthogneiss, marble, and schist (e.g., Guo et al., 1999; Tseng et al., 2006; Tung et al., 2007; Xue et al., 2009). The ca. 900 Ma orthogneiss has a geochemical signature of an active continental magmatic arc, whereas the ca. 800 Ma orthogneiss has geochemical signatures of a rift environment (Tung et al. 2013).

The primary features of the early Paleozoic Qilian orogen include early Paleozoic arc-related granites (e.g., Cowgill et al., 2003; Xiao et al., 2009; Song et al., 2013 and references therein), suture zone rocks, Ordovician and Silurian metamorphic rocks, including ultrahigh-pressure (UHP) rocks in North Qaidam, and a regionally extensive Silurian unconformity overlain by Devonian molasse strata (e.g., Du et al., 2003; Xiao et al., 2009). The Qilian orogen is commonly discussed as involving two suture zones (i.e., the North and South Qilian suture zones in Fig. 1), which may or may not be distinct (e.g., Yin et al., 2007a). The discontinuously exposed North Qilian suture zone consists of ophiolite complexes, high-pressure metamorphic rocks consisting of lawsonite-bearing eclogite and blueschist, volcanic arc rocks, a westward-tapering Silurian flysch strata, and Devonian molasse rocks (e.g., Pan et al., 2004; Song et al., 2006, 2013; Zhang et al., 2007; Xiao et al., 2009; Lin et al., 2010). The South Qilian suture zone links with the North Qinling suture zone in the east

(Yin and Nie, 1996; Tseng et al., 2009; Wu et al., 2016) and consists of serpentinite, altered ultramafic rocks, gabbro, pillow basalt, and mélange with marl and chert (e.g., Yang et al., 2002; Shi et al., 2004; Tseng et al., 2007; Song et al., 2013).

Regional metamorphism, as constrained by Th-Pb monazite ages in synkinematic garnets, U-Pb zircon rim ages, and muscovite $^{40}Ar/^{39}Ar$ ages, began by ca. 480 Ma, and protracted deformation continued until ca. 410 Ma (Qi, 2003; Liu et al., 2006; Lin et al., 2010; Zuza, 2016; Zhao et al., 2017). The related North Qaidam UHP metamorphic rocks involve metamorphism at 490–460 Ma and 440–420 Ma (Mattinson et al., 2007; Menold et al., 2009, 2016; Song et al., 2014).

Although Mesozoic extensional structures and related deposits have been documented around the Qilian Shan region (e.g., Vincent and Allen, 1999; Chen et al., 2003), the dominant structures that define the modern physiography of the Qilian Shan are thrusts and strike-slip faults in the 300-km-wide and 1200-km-long Cenozoic Qilian Shan–Nan Shan thrust belt (Taylor and Yin, 2009; Yin et al., 2008; Zuza and Yin, 2016; Zuza et al., 2016) (Fig. 1). The high topography (~4–5 km) and thickened crust of the Tibetan Plateau have been attributed to lower crustal channel flow (Clark and Royden, 2000) and crustal shortening (Lease et al., 2012) with the possible influence of southward underthrusting of the North China craton (Ye et al., 2015; Zuza et al., 2016).

LITHOLOGY AND STRUCTURAL GEOLOGY OF THE STUDY AREA

The study area is located in the central Qilian Shan (Fig. 1B) and includes the Tuolai Shan Range in the north and the Tuolai Nan Shan Range in the south (Fig. 2). Northwest-trending Cenozoic thrusts in the study area juxtapose older Proterozoic to Mesozoic rocks over younger Mesozoic and Cenozoic strata. We describe the major lithologic units and faults below.

Metamorphic Rocks

The metamorphic rocks are assigned to two units: the older Tuolai Group (unit Pt_1 in Fig. 2) and the younger Tuolai Nanshan Group (Qinghai Bureau of Geology and Mineral Resources, 1991; Pan et al., 2004) (Fig. 3). The Tuolai Group consists of quartzofeldspathic gneiss, mylonitic orthogneiss, mica-garnet schist, metabasite, garnet amphibolites, plagioclase amphibolites, quartzite, and phyllite. Also present in this unit are mylonitic orthogneiss occurring as lenses (1–5 km long and few millimeters to 2 m in thickness) and garnet amphibolite occurring as boundinaged blocks (0.5–5 m wide and 1–3 km long). The younger and relatively lower grade Tuolai Nanshan Group (unit Pt_2 in Fig. 2) consists of mica and garnet schist, quartzite, marble, and locally phyllite and slate. The Proterozoic orthogneiss and granitoid complex (gn in Fig. 2) was mapped in this study as a separate unit from the Tuolai and Tuolai Nanshan Groups (Fig. 3). The foliations of all the metamorphic units are parallel across lithologic contacts, and all units are variably mylonitized. All of these metamorphic rocks are inferred to have Precambrian protolith ages (Qinghai Bureau of Geology and Mineral Resources, 1991; Pan et al., 2004); this is verified by our new geochronology data (discussed in a later section).

The meter- to kilometer-scale eclogite and marble blocks occur as lenses within paragneiss and schist of the Tuolai Group. These eclogite lenses are ~200 m long in the northwest-southeast direction and ~80 m wide in the northeast-southwest direction (Fig. 4). The eclogites appear gray-black to gray-green with massive or banded structures and are partially retrograded to gray-black garnet amphibolite (Zuza, 2016). The paragneiss and schist have strongly developed foliations and stretching lineations. Stretching lineations are observed within the foliation surface, and stretched quartz or plagioclase is most evident in the outcrops. The schist foliation strikes west-northwest and dips 20°NE. The eclogite consists mainly of Na-bearing pyroxenes, amphibole, phengite, quartz, zoisite, and garnet (Figs. 5A–5D). The rims of the eclogite blocks have undergone retrograde metamorphism with pyroxene replaced by amphibole (Figs. 4A, 4B). Petrographic and mineralogical examinations reveal that garnets in this eclogite sample preserved prograde metamorphic zonation in both their element concentrations and mineral inclusions, and the rock belongs to the C-type eclogite classification (Song et al., 2017).

The prograde metamorphic assemblages consist of the biotite, amphibole, and plagioclase inclusions preserved in the garnet core, and prograde pressure-temperature (*P-T*) conditions are estimated to be 568–580 °C and 8.0–8.2 kbar (Fig. 6). Peak metamorphic assemblages are clinopyroxene and coesite pseudomorph inclusions in the mantle part of garnet, and relict rutile in the clinopyroxene + amphibole + plagioclase symplectite. Omphacite is speculated to have also grown in this stage. *P-T* estimates give peak metamorphic conditions of 690 ± 7 °C and 30 ± 3 kbar, which is ultrahigh-pressure (UHP) metamorphism (Fig. 6). The granulite facies retrograde stage is characterized by the amphibole + plagioclase + biotite corona around garnet porphyroblasts. This facies is interpreted to represent an isothermal decompression process at *P-T* conditions of 681–705 °C and 6.8–7.1 kbar (Fig. 6). Continued subsequent retrogression under amphibolite facies conditions is evidenced by coarse-grained matrix amphiboles and *P-T* conditions of 500–545 °C and 3.8–4.3 kbar (Fig. 6). The estimated metamorphic conditions reveal a clockwise *P-T* path (Fig. 6) (Song et al., 2017). The protolith of the eclogite block may have been a tholeiitic basaltic intrusion (Song et al., 2017), possibly a mafic dike intruding the middle to upper crust.

Mélange Complex

A mélange unit consisting of Cambrian–Ordovician pillow basalt, siltstone, metapelite, quartzite, marble, gabbro, and ultramafic rocks (Figs. 2 and 3) is exposed in the northern portion of the mapping area. The unit has been assigned a Cambrian–Ordovician age based on reported fossils (Xiao et al., 1978) and geochronologic studies (Shi et al., 2004; Song et al., 2013; Zuza, 2016). There is significant deformation within the complex, and the lithologic contacts are highly sheared. The Cambrian–Ordovician mélange belt is the segment of a previously documented Yushigou ophiolite belt commonly interpreted as a suture in the Qilian Shan region (Song and Su, 1998; Shi et al., 2004; Hou et al., 2006; Song et al., 2012).

Sedimentary Units

Sedimentary units with ages ranging from Ordovician to Quaternary are distributed throughout the study area (Figs. 2 and 3). Ordovician rocks consist of low-grade metamorphosed sandstone, siltstone, and limestone with minor volcanic rocks. All Ordovician strata are strongly deformed, and the original sedimentary relationships are obscured. Silurian and Devonian strata are absent from the mapping area but are found elsewhere in the Qilian Shan. Silurian rocks are generally considered to represent a flysch basin that transitions into molasse deposits (Du et al., 2003), whereas Devonian rocks are interpreted to represent molasse that was deposited in intermontane and/or foreland basins during the early Paleozoic Qilian orogen (e.g., Xia et al., 2012; Yan et al., 2007).

Carboniferous strata, deposited unconformably on top of the mélange complex and metamorphic rocks (Figs. 2, 3, and 4G), are composed of conglomerate, quartz arenite, arkosic sandstone, and siltstone. This unit is juxtaposed against Permian strata by a thrust in the northern part of the study area (Figs. 2 and 4H). The Permian unit, composed mostly of

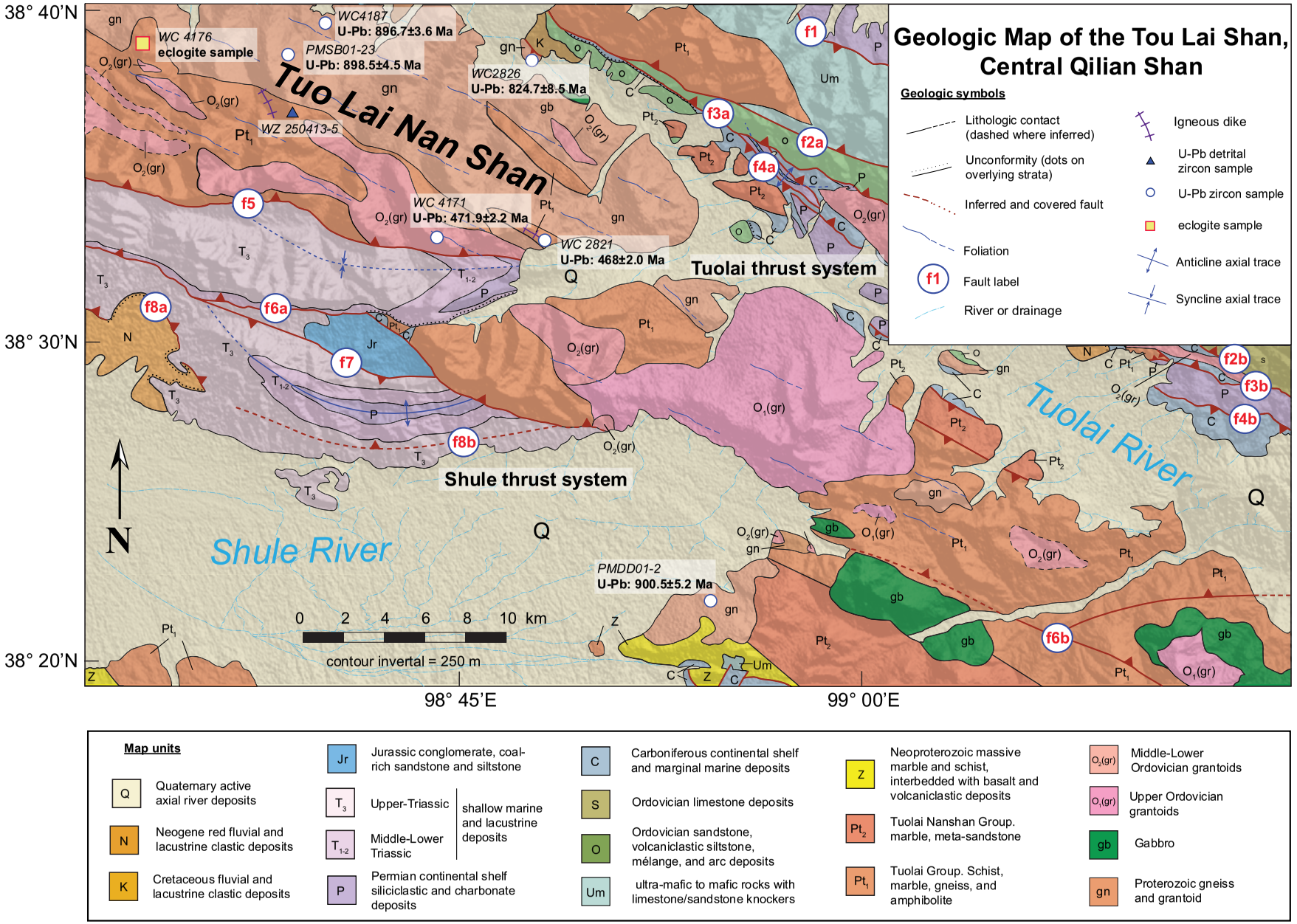

Figure 2. Geologic map of a region in the central Qilian Shan–Nan Shan thrust belt produced for this study. Underlying base map is from www.gscloud.cn.

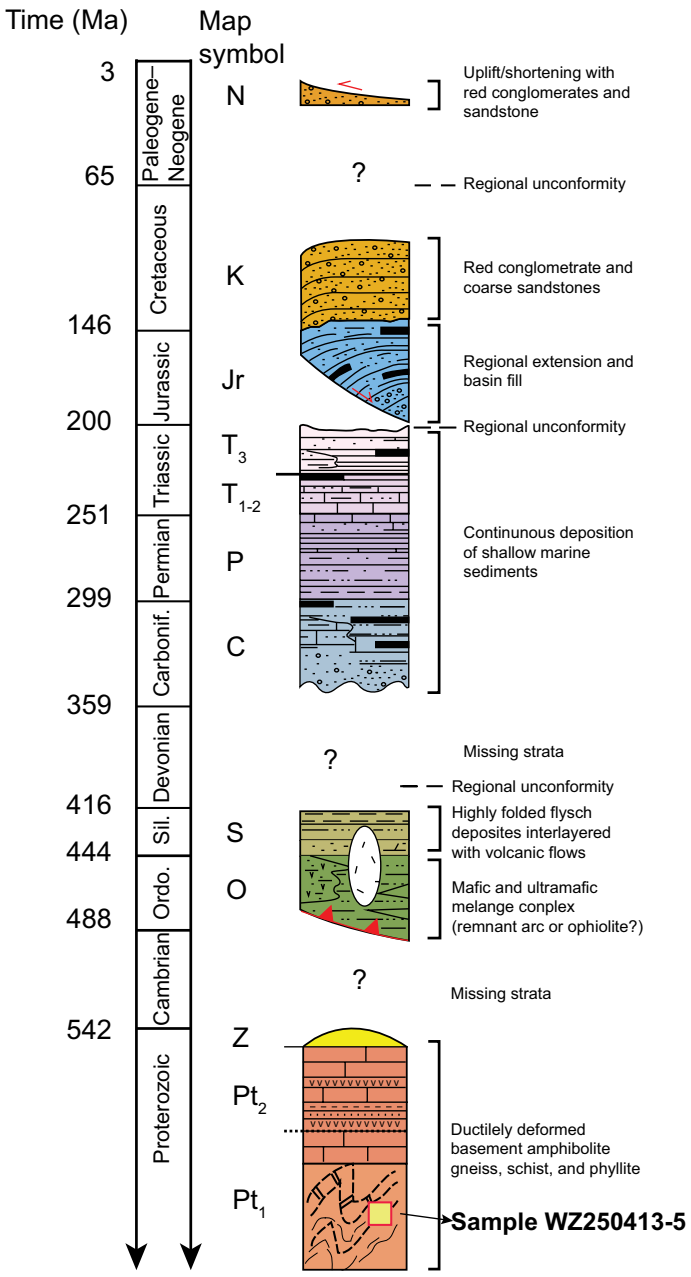

Figure 3. Tectonostratigraphic sections of the central Qilian Shan–Nan Shan thrust belt produced from this study. Ordo.—Ordovician; Sil.—Silurian; Carbonif.—Carboniferous.

arkosic sandstone, is conformably overlain by lower to upper Triassic interbedded arkosic sandstone, siltstone, and shale (Fig. 3) (Wu, 2013).

Jurassic strata are exposed in the central part of the mapping area where their base is defined by a conformable contact with the underlying upper Triassic sequences (Fig. 2). The lithology of the Jurassic unit consists of interbedded quartz arenite, siltstone, and coal-bearing shale (Fig. 3). The Cretaceous strata are composed of polymictic conglomerate and pebble sandstone (Fig. 3). The unit is only exposed along the northern margin of the mapped area.

Neogene sedimentary rocks are exposed only in the southern part of the study area along the margins of intermontane basins, and are juxtaposed by thrusts below Triassic units in the west and Carboniferous strata in the east (Figs. 2 and 4). The Neogene unit consists of interbedded fine-grained sandstone and muddy limestone with resistant conglomerate marker beds (Fig. 3). Quaternary sediments include fluvial, glaciofluvial, and lacustrine deposits (Fig. 2).

Igneous Rocks

Several large (10–50 km^2) and many minor (1–10 km^2) nonfoliated granitoids intrude the Proterozoic strata, gneiss complex, and the Ordovician strata, but are unconformably overlain by Carboniferous and younger strata (Fig. 2). This relationship places an early Paleozoic age limit to the plutonism timing, which must be older than Carboniferous. The compositions of the plutons range from granite to quartz-monzonite with variable amounts of potassium and plagioclase feldspar. One of the plutonic bodies had a reported whole-rock K-Ar age of 345 ± 17 Ma (Qinghai Bureau of Geology and Mineral Resources, 1991), but new zircon data suggest a crystallization age of ca. 450 Ma (Zuza, 2016). The Ordovician granitoids are mapped as O_2 (gr) (Fig. 2) in the central part of the mapping area, and outcrops range in size from tens of to a few square kilometers. These granitoids range in composition from alkali feldspar granite to quartz monzonite and intrude basement rocks and the contact between the Proterozoic and early Paleozoic strata (Fig. 2). Our geochronology results indicate that this pluton crystallized at ca. 472 Ma (sample WC4174).

The foliated granitoid bodies in the northern part of the study area are mostly mylonitized along their southern margins and intrude Proterozoic metamorphic rocks (Fig. 2). The shear zone is 30 m wide and dips to the south. Foliations are all near vertical and northwest-striking, and stretching lineations generally have a northwest trend and are subhorizontal (Fig. 4D). Kinematic indicators, including S-C fabrics and mantled porphyroclasts, suggest right-lateral shear of this entire unit (Figs. 5E, 5F). Because the different metamorphic units (e.g., schist, amphibolite, and foliated granitoid) all have parallel foliations and stretching lineations (Fig. 4D), it is likely that the same deformational event affected the units together. The mylonitized pluton does not display a postemplacement subsolidus gneissic foliation. Geochronology results presented in Zuza (2016) indicate that this foliated granitoid located in the northern part of the study area has a crystallization age of 950–900 Ma, which places a lower age bound on the protolith of the metamorphic complex it intrudes. Our new U-Pb zircon ages suggest the existence of granitoid bodies with a crystallization age of ca. 825 Ma (sample WC2826) in the northwest part of the Tuolai River (Fig. 2).

Structural Geology

The primary structures in the map area are the Cenozoic range-bounding Shule thrust system in the south and the Tuolai thrust system in the north (Fig. 2). The fault systems are separated by a mylonitic gneiss complex in the central study area that is the exposed hanging wall of the Shule thrust system (Fig. 2). These faults, which are labeled f1 through f8 from north to south, respectively (Fig. 2), are discussed below.

Tuolai Thrust System

The Tuolai thrust system is exposed along the northern margin of the study area and is composed of four primary fault strands (Fig. 2). The structural trend of the Cenozoic thrusts parallels the early Paleozoic contact between the Tuolai Group and Ordovician mélange (Fig. 2). Northwest-striking thrusts in both the Tuolai and Shule thrust systems place metamorphic basement rocks over early Paleozoic–Mesozoic and Cenozoic strata. This relationship is speculative because our mapped

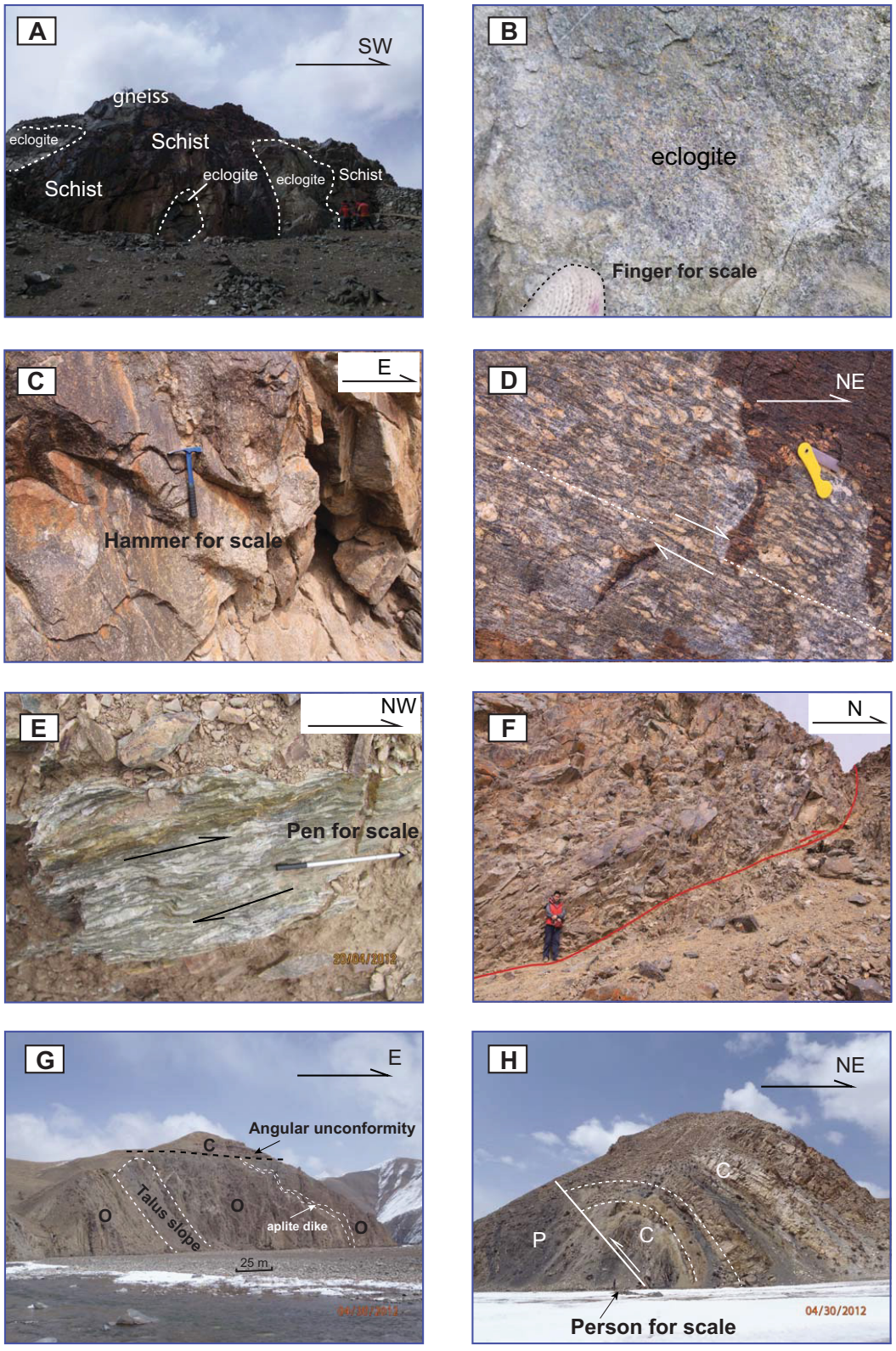

Figure 4. Field photographs and annotations. (A, B) Field occurrence of an eclogite block. (C) Field occurrence of plagiogneiss. (D) Field occurrence of the studied mylonitic orthogneiss sample. Photo shows a right-slip shear in the metamorphic unit. (E) Field occurrence of plagiogneiss showing a right-slip shear zone in this metamorphic unit. (F) Field occurrence of the metaporphyritic diorite sample. The fault shows top-to-the-north displacements with downdip stretching lineations. (G) Angular unconformity between nearly horizontal Carboniferous rocks and vertically foliated Ordovician rocks below. (H) Hanging-wall anticline above fault f4a.

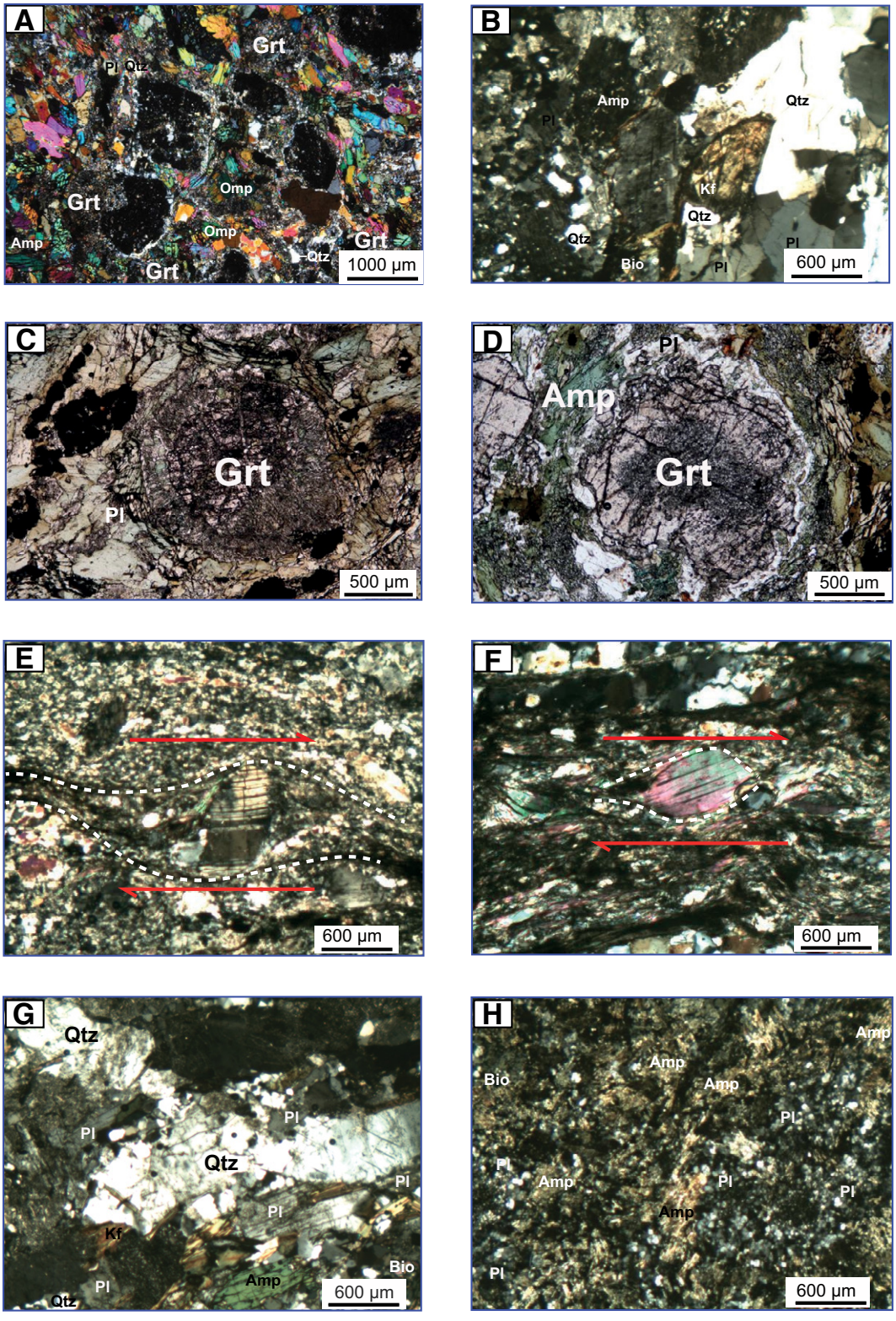

Figure 5. Photomicrographs of representative petrographic characteristics and mineral assemblages of representative metamorphic rocks from the central Qilian Shan. (A) The eclogite block. (B) Metaporphyritic diorite sample. (C) Garnet is surrounded by wormlike intergrowths of the eclogite sample. (D) Metasomatism developed between garnets and plagioclase-amphibole aggregates. (E) Foliations in an S-C tectonite of the studied mylonitic orthogneiss sample. (F) The S-foliation of the studied mylonitic orthogneiss sample is defined by the preferred orientation of large mica grains, called mica porphyroclasts (or fish), and by a grain-shape foliation in the quartz. (G) Plagiogneiss sample. (H) Plagioclase amphibolites sample. Grt—garnet; Amp—amphibole; Pl—plagioclase; Qtz—quartz; Bio—biotite; omp—omphacite; Kf—potassium feldspar.

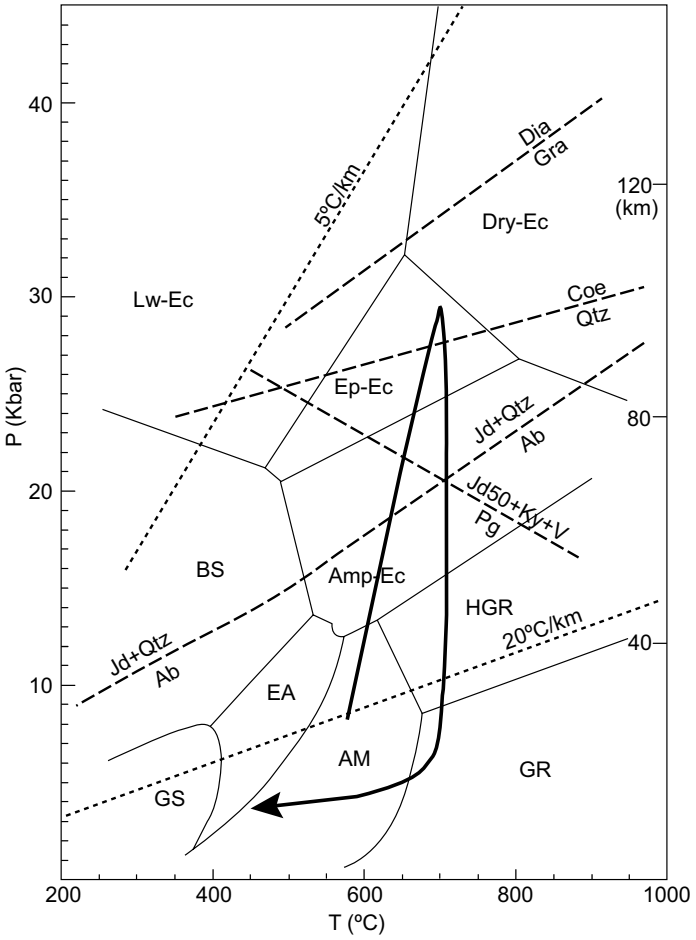

Figure 6. Pressure-temperature (*P-T*) path of the eclogite block in the central Qilian Shan. Data are from Song et al. (2017). *P-T* intervals of metamorphic facies modified after Liou et al. (1998, 2009). Dia—diamond; Gra—graphite; Ep—epidote; Ec—eclogite; Coe—coesite; Qtz—quartz; Lw—lawsonite; BS—blueschist; Jd—jadeite; Amp—amphibole; Ab—albite; GS—greenschist; EA—epidote amphibolite; AM—amphibolite; GR—granulite.

region does not contain faults that link to both the Tuolai and Shule thrust systems. For convenience of description, the Tuolai thrusts are labeled f1 through f4, from north to south, respectively (Fig. 2). Fault f1 is a south-dipping thrust at its central segment where it places ultramafic rocks (i.e., fragments of the Yushigou ophiolite; e.g., Hou et al., 2006; Song et al., 2013) over north-dipping Permian strata.

Fault f2 is the largest throughgoing fault in the northern of Tuolai Nan San (Fig. 2). Along its eastern segment (i.e., fault f2a in Fig. 2) the fault cuts the ultramafic unit (unit Um in Fig. 2) unit in the north and the Ordovician mélange unit in the south (Fig. 2). Northwestward along strike fault f2a juxtaposes rocks of the Tuolai Group (Pt_1 in Fig. 2) in the hanging wall over the Ordovician mélange unit and south-dipping Carboniferous (unit C in Fig. 2) and Cretaceous strata in the footwall (unit K in Fig. 2). The relationship between the Tuolai Group complex and ultramafic rocks is unknown due to inaccessibility of higher elevation regions. Fault f2b juxtaposes the Silurian mélange unit in the north against the Carboniferous unit in the south (Fig. 2).

Fault f3 is a north-dipping thrust fault that branches from fault f2a (Fig. 2). The hanging wall consists of the Ordovician mélange unit in which both bedding and north-dipping cleavage strike parallel to the fault zone. Fault scarps across alluvial fans are evident in the northeastern part of the study area (Fig. 2), indicating that the fault is still active.

Thrust fault f4a branches off fault f3a and extends to the southeast (Fig. 2). The hanging wall of fault f4a consists mostly of Carboniferous strata thrust over the Permian strata. In the east, fault f4b juxtaposes Carboniferous strata in the hanging wall over Permian strata in the footwall.

Shule Thrust System

The northwest-striking Shule thrust system is along the southern edge of the Tuo Lai Nan Shan (Fig. 2). This system consists of several fault strands that merge with one another along strike to the west or die out into folds to the northwest and in the western part of the study area. We informally name the faults in the Shule thrust system f5, f6, f7, and f8 sequentially from north to south (Fig. 2). The Shule thrust system is composed of both north- and south-dipping thrusts. A south-dipping fault (fault f7 in Fig. 2) is truncated by north-dipping faults and are covered in some regions by younger strata (Fig. 2), requiring them to be the backthrusts of the north-dipping thrusts in the system. North-directed thrusts are thin-skinned, rooting in Permian or younger strata, whereas south-propagating thrust faults root into the gneiss complex (Fig. 2) and are responsible for the large exposure of crystalline basement rocks. All major thrust faults in the Shule thrust system are associated with folds within the Permian and Triassic strata (Fig. 2). Out-of-sequence thrusting suggests the development of folding prior to thrusting (Fig. 2).

Fault f5 marks the northern edge of the Shule thrust system and is within the Tuolai Group in the east but cuts upsection of the footwall Triassic strata to the west (Fig. 2). This juxtaposition relationship implies that the stratigraphic throw across the fault increases from east to west. The footwall of fault f5 exposes a westward-plunging and northward-overturned syncline (in Fig. 2) within the Triassic strata.

Fault f6 is the most laterally continuous fault in the study area. In the east of Figure 2 fault f6b is within the Tuolai Group. Cleavage is well developed in the middle-lower Triassic strata directly north of the fault. In the eastern part of fault f6a, the fault places a plutonic body and the Tuolai Group over Permian and Triassic strata (Fig. 2). There, the fault also truncates an anticline cored by Permian strata in its footwall (Fig. 2). Across the central segment of fault f6a, it places Triassic strata over Triassic and Jurassic strata. The fault also truncates a major unconformity between Carboniferous in the east and Middle Triassic strata in the west in the hanging wall (Fig. 2). Along the western segment of fault f6a the fault places Triassic over Jurassic strata.

Fault f7 dips to the south and terminates at fault t f6a in the east and west. The fault cuts downsection in the footwall from Jurassic strata in the east to Triassic strata in the west. In contrast, the same fault cuts upsection in the hanging wall from middle-lower Triassic to upper Triassic strata from east to west. The fault truncates the western end of the anticline in the west and the anticline's northern limb in the east (Fig. 2).

Fault f8 is observed at its eastern end, which dips to the northeast and placing north-dipping Triassic beds over south-dipping Neogene strata (Fig. 2). Kilometer-scale folds are observed in the hanging wall of this fault, exposing Permian–Triassic rocks. Although no direct fault kinematic measurements were made for this fault, the fold axes are parallel to the fault strike, which may suggest that this fault is primarily a dip-slip structure.

DATA COLLECTION AND ANALYTICAL METHODS

Eight samples were selected for U-Pb zircon geochronology analysis, including one deformed orthogneiss sample from the early Paleozoic

Qilian arc, O_2 (gr), one plagioclase amphibolite dike sample from the metamorphic basement, one eclogite block sample from the northwestern part of this study area, one schist sample from the Tuolai Group with a Proterozoic depositional age, and four foliated granitoid samples from the metamorphic basement (Table 1). Representative cathodoluminescence (CL) images of zircons dated in this study are shown in Figure 7. Concordia diagrams of single zircon analyses and relative probability plots of the ages are shown in Figures 8 and 9. Five foliated granitoid samples from the metamorphic basement were collected for whole-rock geochemical analysis. Detailed analytical methods are provided in the text section in the GSA Data Repository Item[1].

TABLE 1. SUMMARY OF SAMPLES AND SAMPLE LOCATIONS

Sample	Description	Lat (°N)	Long (°E)
WC4171	mylonitic orthogneiss	38.50	98.75
WC4173	eclogite block	38.60	98.57
WC4187	plagiogneiss	38.64	98.68
PMDD01-2	plagiogneiss	38.26	98.90
PMSB01-23	plagiogneiss	38.59	98.64
WC2826	metaporphyritic diorite	38.59	98.80
WZ250413-5	schist	38.55	98.65
WC4181	quartzite	38.58	98.65
WC2821	plagioclase amphibolites	38.48	98.83

Note: All samples dated by U-Pb zircon method. Data from our study.

Sample Description

Eclogite Blocks (Sample WC4173)

Our eclogite sample consists of euhedral orthopyroxene, clinopyroxene, plagioclase, brown amphibole ± rutile, ± biotite, ± apatite, ± opaque minerals (ilmenite and magnetite), that preserves igneous textures when coarse grained. Textural relationships do not allow us to reconstruct a clear crystallization order. Amphibole is generally concentrated in millimeter to centimeter bands. Large (15–50 μm in diameter) orthopyroxenes occur around opaques, apatites, and clinopyroxenes. Biotite is rare and occurs as deformed flakes within plagioclase or between plagioclase and pyroxene. Microdomains of different composition corresponding to the original igneous minerals were preserved during metamorphism, and the large euhedral crystals have recrystallized rims. The modal abundance of garnet varies from 55 to 60%, hornblende from 20 to 25%, clinopyroxene from 10 to 15%, plagioclase ~5%, quartz from 4 to 5% and mica ~1% (Fig. 5A). Garnet grains are surrounded by the wormlike intergrowths of plagioclase (Fig. 5C), and metasomatism is developed between the garnets and plagioclase-amphibole aggregates (Fig. 5D).

Mylonitic Orthogneiss (Sample WC4171)

The analysis presented here is focused on the ductile to brittle-ductile deformation of the mylonitic orthogneiss in the Tuolai Group. As in other ductile shear zones in the Qilian orogen (Qi, 2003), the mylonitic gneiss complex is not a discrete surface but a zone of highly deformed rocks as wide as several kilometers. Layers (few millimeters to 2 m in thickness) of mylonitic orthogneiss have well-developed stretching lineations (Fig. 4D). The upper 1500 m of mylonitic orthogneiss consist mainly of quartz (68%), K-feldspar (12%), plagioclase (5%), biotite (5%), and muscovite (10%). Shear deformation resulted in a well-defined compositional banding of alternating pure quartz and fine-grained feldspar-phyllosilicate–rich layers. These layers anastomose around less deformed feldspar augen. Recrystallization is mainly by growth of new grains along the edge of feldspar grains or along fractures. Some feldspar porphyroclasts show deformation in the form of patchy undulose extinction or deformation twinning (Figs. 5E, 5F). Larger grains (30–55 μm in diameter) are mainly fractured by synthetic and antithetic shear fractures. Retrogressive alteration of feldspar to muscovite and quartz is common and may be associated with the cooling of the related shear zone. Quartz has undergone extensive dynamic recrystallization by subgrain rotation and grain boundary migration (Fig. 5E). Pure quartz layers show both shape- and lattice-preferred orientations (Figs. 5E, 5F).

Foliations are defined by weak to strong mineral alignment (mostly mica and amphibole grains). Stretching lineations are observed within the foliation surface, and stretched plagioclase is evident in many outcrops. Stretching lineations are subhorizontal and trend to the southeast. Abundant shear-sense indicators were observed in the surface perpendicular to foliation and parallel to the stretching lineations, including mantled porphyroclasts, oblique foliation, stair stepping, S-C tectonites (Fig. 5E), mica fish (Fig. 5F), lattice-preferred orientation of quartz, and antithetic and synthetic microfaults in feldspar grains. These features reveal a noncoaxial deformation history with apparent right-lateral kinematics parallel to the southeast-trending subhorizontal stretching lineations (Fig. 4D). At the base of fault f2, the transition to the footwall shows a strong cataclastic overprint. The orientation of striation on slickensides is roughly parallel to the mylonitic stretching lineation (Fig. 4D), indicating a constant shear direction during the transition from ductile to brittle deformation.

Plagioclase Amphibolite (Sample WC2821)

This sample was collected along the Tuolai River from part of a 1–3-km-long and 0.5–5-m-wide slightly deformed to undeformed amphibolite dike that intrudes the Proterozoic schist unit (i.e., Pt_1; Fig. 2). The plagioclase amphibolite sample consists mainly of plagioclase (≥45%), amphibole (50%–55%), and ~5% biotite (Fig. 5H).

Plagiogneiss (Samples WC4187, PMDD01–2, and PMSB01–23)

The plagiogneiss occurs as lenses that intrude the surrounding Tuolai Group schist (Figs. 4C, 4E). It appears gray-white to light beige and has well-developed gneissic foliations defined by medium-grained biotite and muscovite. The rocks strike approximately west-northwest and dip 80°N. The medium-fine grained plagiogneiss sample consists of plagioclase (35%–40%), K-feldspar (10%–15%), quartz (35%), amphibole (10%), and biotite (5%) (Fig. 5G). The Ordovician plutonic bodies intrude the plagiogneiss gneiss (Fig. 4C).

Metaporphyritic Diorite (Samples WC2826 and WC2826–2)

The metaporphyritic diorite has a strong foliation and well-developed augen structure (Fig. 4F). The Ordovician gabbro intrudes into the metaporphyritic diorite body. The fine-grained metaporphyritic diorite appears gray-white to light-flesh-colored with a porphyritic structure. The phenocrysts are mainly of plagioclase (5%), and the substrates consist of plagioclase (50%), K-feldspar (20%), quartz (10%), amphibole (10%), and biotite (5%) with a 0.1–0.9 mm grain size (Fig. 5B).

Schist Sample (Sample WZ250413–5)

This schist sample has a well-developed schistose structure. The sample domains bounded by the foliation planes consist mostly of quartz and feldspar grains that display straight crystal edges as a result of

[1]GSA Data Repository Item 2017231, the detailed methods of U-Pb zircon geochronology and geochemical analyses of igneous rocks in this study, and Table DR1: LA-ICP-MS results for zircons U-Pb ages of Qilian samples in this study, is available at http://www.geosociety.org/datarepository/2017, or on request from editing@geosociety.org.

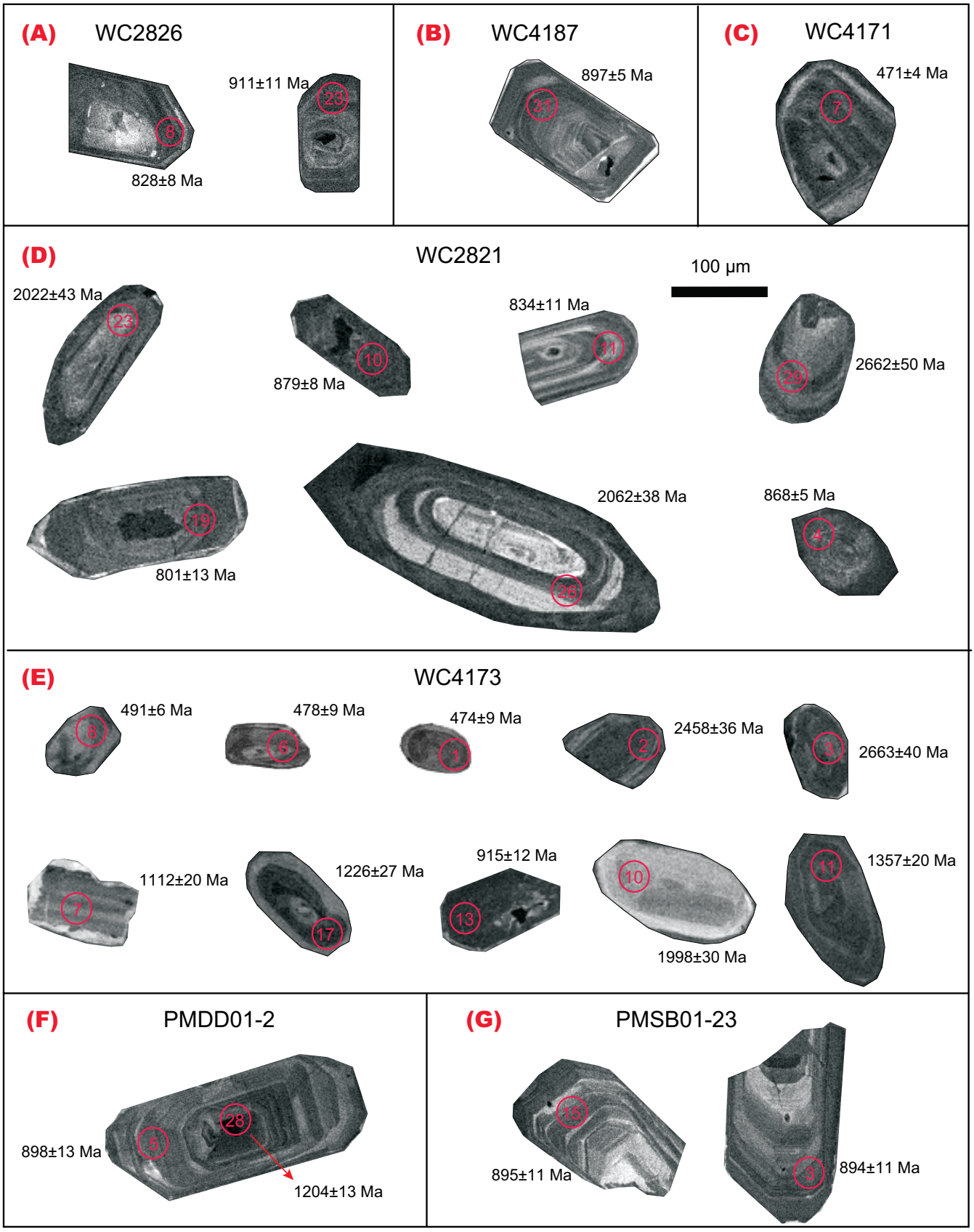

Figure 7. Representative cathodoluminescence images of zircons dated in this study. Red numbered circles are analyzed spots for U-Pb dating.

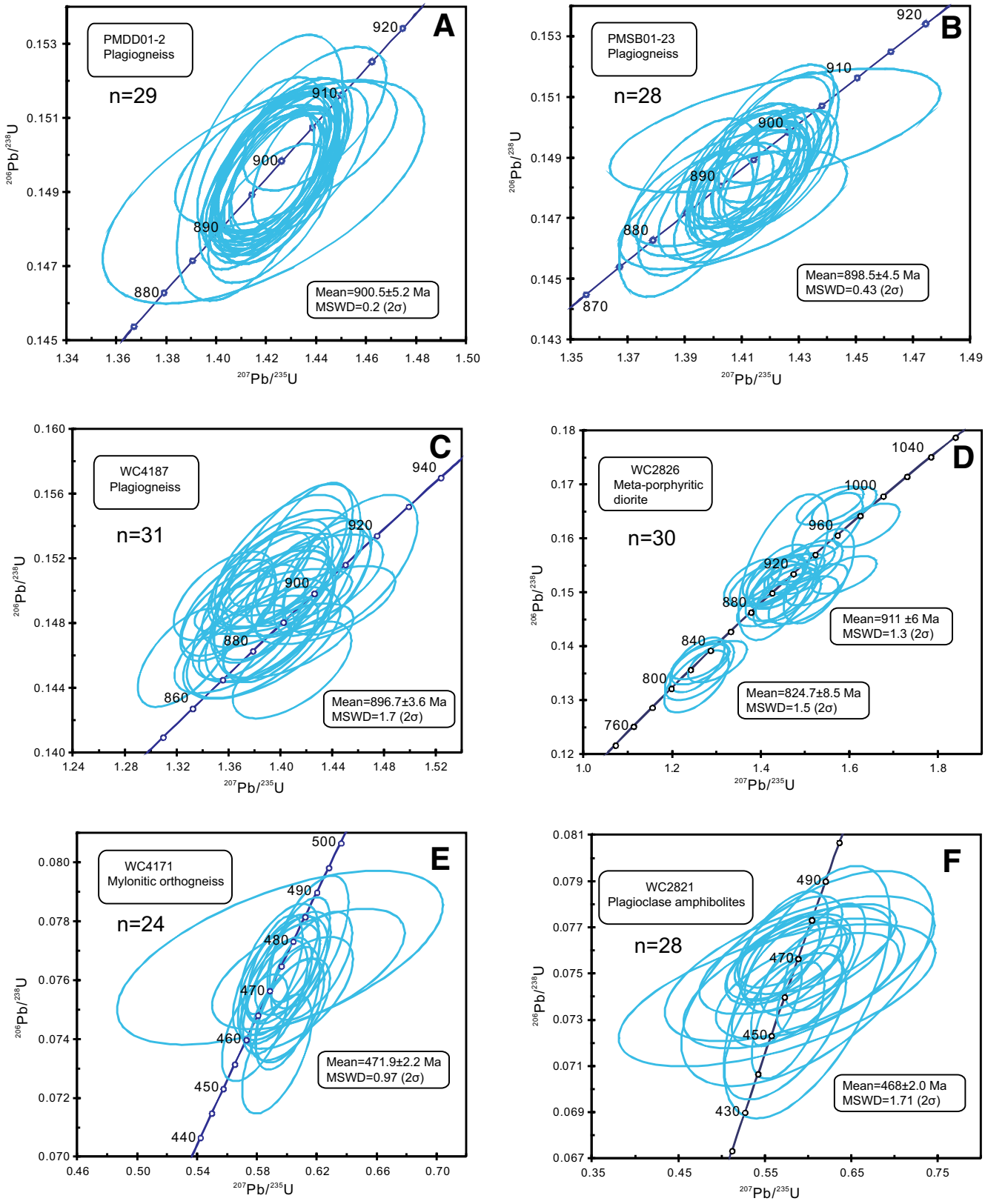

Figure 8. Zircon concordia diagrams of granitoid samples collected. MSWD—mean square of weighted deviates. (A) Sample PMDD01–2: 901 ± 5 Ma crystallization age is obtained from 28 analyses. (B) Sample PMSB01–23: 899 ± 5 Ma crystallization age is obtained from 28 analyses. (C) Sample WC4187: 897 ± 4 Ma crystallization age is obtained from 31 analyses. (D) Sample WC2826: 825 ± 9 Ma crystallization age is obtained from 30 analyses. (E) Sample WC4171: 472 ± 2 Ma crystallization age is obtained from 30 analyses. (F) Sample WC2821: 468 ± 2 Ma crystallization age is obtained from 24 analyses.

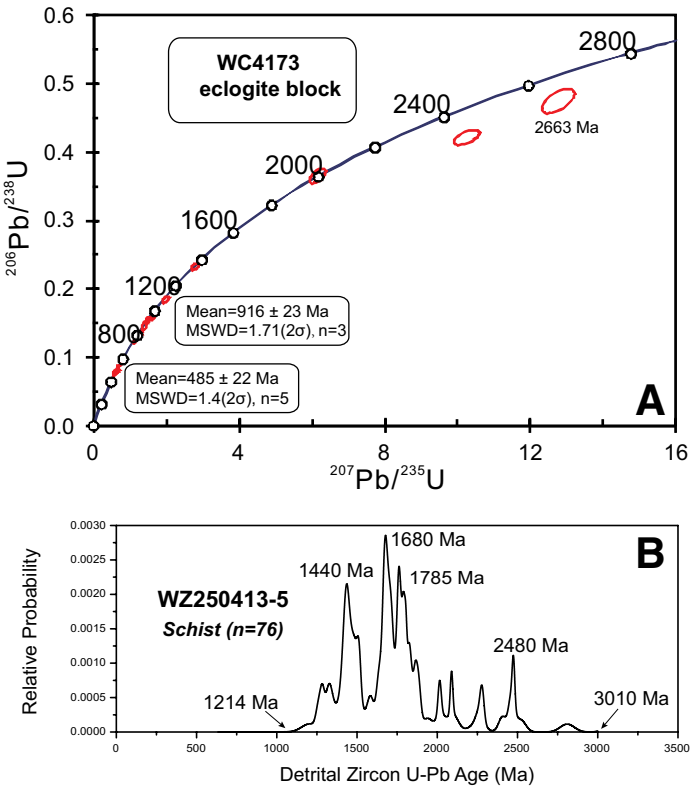

Figure 9. (A) Zircon concordia diagrams showing results for the eclogite sample (WC4173). MSWD—mean square of weighted deviates. (B) Relative probability plot of zircon U-Pb ages (Ma) for the schist sample WZ250413-5 from the central Qilian Shan.

recrystallization. The schist sample consists of plagioclase (20%), quartz (50%), muscovite (20%), and biotite (10%).

GEOCHRONOLOGY RESULTS

The analytical data from U-Pb zircon dating are presented in Table DR1. The fractionation correction and results were calculated using GLITTER 4.0 (Macquarie University, Sydney, Australia, http://www.glitter-gemoc.com/Glitter-444_p_12.html), and common Pb was corrected following the method described by Andersen (2002). Zircon grains chosen for this study (exception of eclogite sample WC4171) were euhedral, prismatic in shape, and ~100–150 μm long. The length to width ratios of dated zircon grains were typically 2:1–3:1. A few grains show elongate length:width ratios of 4:1. Most of the dated zircon grains were transparent and colorless under the optical microscope, although some appeared brownish, possibly due to high U contents. Zircon grains display both concentric zoning and inherited cores with magmatic overgrowth rims (Fig. 7). Uncertainties of individual analyses are reported with 1σ errors; weighted mean ages are reported at the 2σ confidence level. Age calculations and concordia plots were made using Isoplot (Ludwig, 2003). In total, 263 zircons were analyzed, and the analytical results are presented in Figures 8 and 9. Most analyses are concordant or nearly concordant, clustering as single age populations. To eliminate the effects of radiation damages (typically displayed by dark CL images indicating high U contents), Pb loss, and erroneous analyses, we used only the ages that clearly belonged the same Gaussian distribution for calculating the weighted mean ages of pluton emplacement (Fig. 7) (e.g., Wu et al., 2016). The interpreted ages are based on $^{206}Pb^*/^{238}U$ ages for grains younger than 1000 Ma and $^{207}Pb^*/^{206}Pb^*$ ages for grains older than 1000 Ma (Ludwig, 2003). Our goal was to use these analyses to determine the crystallization ages of the plutonic bodies and detrital zircon ages from the schist. Although the Th/U ratios and crystal morphology (Fig. 7) suggest that all zircon grains have a magmatic origin (Harley et al., 2007), there are a few zircons that have anomalously low Th/U ratios (<0.1).

Eclogite Block (Sample WC4173)

Most of the CL images of zircons from eclogite sample show low luminous intensity, no zoning, weak zoning, or spongy zoning with an ~5-μm-wide strong CL belt at edges, indicating that most of them are metamorphic or inherited zircons (Fig. 7E). We analyzed 17 spots from 17 zircon grains from this sample. Apparent zircon ages range from 474 Ma to 2663 Ma, with two minor peaks at 485 Ma and ca. 916 Ma (Fig. 9A); 5 analyses on subhedral grains with lamellar or oscillatory zoning yielded a $^{207}Pb^*/^{206}Pb^*$ weighted mean age of 916 ± 23 Ma (mean square of weighted deviates, MSWD = 1.71). Four recrystallized zircon rims (Fig. 7E) have late Cambrian–Early Ordovician $^{206}Pb/^{238}U$ ages with a weighted mean age of 485 ± 22 Ma (MSWD = 1.4) (Fig. 9A), which we suggest represents the eclogite facies metamorphic age. Three zircon cores with oscillatory or weak zoning yielded Paleoproterozoic–Neoarchean $^{207}Pb/^{206}Pb$ ages of ca. 1998 Ma, ca. 2458 Ma, and ca. 2663 Ma (Figs. 7E and 9A). The inherited zircon ages older than 1.0 Ga are discordant and fail to define a discordia line (Fig. 9A), but these data indicate the presence of Precambrian crystalline rocks in the central Qilian Shan. This also shows that the protolith of the eclogite either contains detrital zircon grains or intruded through Precambrian continental crust.

Metaporphyritic Diorite (Sample WC2826)

The zircon rims of 30 grains were analyzed, and all 30 spots yield concordant $^{206}Pb/^{238}U$ ages that range from 808 Ma to 990 Ma (Fig. 8D). There are two dominant age populations: the younger population, which accounts for ~20% of the analyzed grains, has a peak age of ca. 825 Ma, whereas the older population has a peak age of ca. 911 Ma (Fig. 8D). We interpret the younger weighted mean age of multiple rim analyses of 824.7 ± 8.5 Ma (MSWD = 1.5) to represent the crystallization age of the diorite sample. The weighted mean age of the older population is 911 ± 6 Ma, which we interpret to reflect inherited zircon grains (Figs. 7A and 8D).

Plagiogneiss (Sample WC4187)

Analyses of 31 spots from 31 zircon grains yield concordant $^{206}Pb/^{238}U$ ages varying from 873 Ma to 914 Ma (Fig. 8C), with a weighted mean age of 896.7 ± 3.6 Ma (MSWD = 1.7). We interpret this to represent the crystallization age of the Neoproterozoic granitoid (Figs. 7B and 8C).

Plagiogneiss (Sample PMDD01–2)

We analyzed 29 zircon grains from this sample. All 29 spots yielded similar ages with apparent $^{206}Pb/^{238}U$ ages of varying from 892 Ma to 906 Ma, except for one analysis that yielded a zircon age of 1203 Ma. The analyses are concordant and combine to a weighted mean age of 900.5 ± 5.2 Ma (MSWD = 0.2), which we interpret to represent the crystallization age of the granitoid (Figs. 7F and 8A).

Plagiogneiss (Sample PMSB01–23)

Analyses of 28 spots on 28 zircon grains yielded similar concordant $^{206}Pb/^{238}U$ ages varying from 886 Ma to 902 Ma, except for one zircon grain with an age of 954 Ma (Fig. 8B). These analyses produce a weighted mean age of 898.5 ± 4.5 Ma (2σ), which may represent the crystallization age of the granitoid (Figs. 7G and 8B).

Mylonitic Orthogneiss (Sample WC4171)

Analyses of 24 spots on 24 zircon grains yielded similar concordant ages varying from 445 Ma to 507 Ma (Fig. 8E), with a weighted mean age of 471.9 ± 2.2 Ma (MSWD = 0.97). We interpret this to represent the Early Ordovician crystallization age of the granitoid (Figs. 7C and 8E).

Plagioclase Amphibolite (Sample WC2821)

We analyzed 28 spots on 18 different zircon grains. Most analyses (~75%) yielded concordant Ordovician ages ranging from 452 Ma to 474 Ma (Fig. 8F), but spots 10, 11, 19, 23, 26, and 29 yielded much older Proterozoic ages (Fig. 7D). The weighted mean age of the Ordovician grains is 468 ± 2 Ma (MWSD = 1.71), which we interpret to represent the crystallization age of the granitoid. The older grains are probably inherited zircons from Neoproterozoic and Neoarchean to Paleoproterozoic crustal sources (Fig. 7D).

Schist (Sample WZ250413–5)

This sample was collected from the quartzofeldspathic schist in the Taolai Group that is penetratively deformed by the development of crenulation cleavage, and the rock sample underwent amphibolite-grade metamorphism (see *P-T* estimates in Zuza, 2016). We analyzed 76 detrital zircon grains. A grain with an age of ca. 1203 Ma is the youngest grain of this schist sample. The weighted mean age of the three youngest grains with overlapping ages is 1214 Ma. In addition to a prominent ca. 1700 Ma age peak, two other age peaks are centered at 1432 and 2478 Ma, and the oldest zircon has an age of ca. 3010 Ma (Fig. 9B).

GEOCHEMICAL ANALYSES OF IGNEOUS ROCKS

Major and Trace Element Compositions of the Plagiogneiss and Metaporphyritic Diorite Samples

Three plagiogneiss samples (samples WC4187, PMDD01–2, and PMSB01–23) and two metaporphyritic diorite samples (samples WC2826–1 and WC2826–2) were analyzed for major and trace element compositions (Table 2). The plagiogneiss samples are classified as granite on the (K_2O + Na_2O) versus SiO_2 plot (Middlemost, 1994), whereas the metaporphyritic diorite samples are classified as granodiorite (Fig. 10A). In the A/NK versus A/CNK diagram (Maniar and Piccoli, 1989), these rocks are peraluminous (molar A/CNK = 1.06–1.22 and A/NK = 1.27–1.74; Fig. 10B).

Analytical results of trace element measurements are summarized in Table 2. For the metaporphyritic diorite samples, the multi-element diagram normalized to the primitive-mantle composition shows enrichment in large ion lithophile elements and depletion in high field strength elements (Fig. 10C). The rare earth element (REE) abundances normalized by chondrite values of Sun and McDonough (1989) vary from sample to sample. All samples display enriched light REE and flat heavy REE profiles without distinct Ce anomalies (Figs. 10C, 10D). The most prominent difference in the REE abundance plot between the ca. 900 Ma plagiogneiss samples and ca. 820 Ma metaporphyritic diorite samples is that the younger samples display a strong negative Eu anomaly whereas the older samples display more subdued negative Eu anomalies (Figs. 10C, 10D). The negative Eu anomalies are commonly associated with removal of plagioclase from felsic melts during crystal fractionation (e.g., Rollinson, 2014).

The early phase granitoids, including the ca. 900 Ma plagiogneiss samples, plot in the I- and S-type granite fields that are commonly associated with arc magmatism and/or crustal anataxis (e.g., Whalen et al., 1987; Eby, 1990, 1992; Turner et al., 1992) (Figs. 9E, 9F). In contrast, the later phase granitoids, including the ca. 820 Ma metaporphyritic diorite samples, plot in the field of A-type granites (Fig. 10E, 10F), which are generally associated with extension regardless of the origin of the magma source (e.g., Whalen et al., 1987; Eby, 1990, 1992; Turner et al., 1992). Discrimination diagrams allow further refinement of the assigned tectonic environments of the two phases of Neoproterozoic granitoids from the basement of the central Qilian Shan. In the Nb versus Y diagram (Pearce et al., 1984; Pearce, 1996), the ca. 900 Ma plagiogneiss samples plot in the triple junction region of the volcanic arc, collision orogen, and the within-plate fields, whereas the ca. 820 Ma metaporphyritic diorite samples plot mostly in the within-plate field (Fig. 10G). In the Rb versus Y + Nb

TABLE 2. MAJOR AND TRACE ELEMENTS FOR THE PLUTONIC SAMPLES FROM THE CENTRAL QILIAN SHAN

Samples	WC2826	WC2826-2	PMDD01-2	PMSB01-23	WC4187
Major element (wt%)					
SiO_2	71.95	69.04	76.06	69.63	73.08
Al_2O_3	13.23	13.49	12.49	14.71	13.86
TiO_2	0.36	0.57	0.22	0.54	0.19
Fe_2O_3	0.83	1.60	0.17	0.70	0.85
FeO	2.33	3.15	1.39	3.16	1.00
CaO	1.11	1.80	0.75	2.98	0.81
MgO	0.47	0.71	0.30	0.77	0.39
K_2O	5.52	4.42	4.78	2.90	5.67
Na_2O	2.38	2.42	2.83	3.24	2.30
MnO	0.04	0.07	0.02	0.04	0.06
P_2O_5	0.09	0.15	0.14	0.16	0.09
H_2O^+	1.00	1.42	0.72	0.60	1.30
LOI	0.54	1.24	0.67	0.38	1.17
K_2O + Na_2O	7.90	6.84	7.61	6.14	7.97
A/CNK	1.11	1.12	1.12	1.06	1.22
A/NK	1.34	1.54	1.27	1.74	1.40
Trace element (ppm)					
Y	64.70	89.60	50.00	11.60	11.00
La	91.50	48.30	27.10	57.00	18.20
Ce	170.00	96.60	59.40	111.00	37.00
Pr	20.50	13.10	6.83	12.00	4.23
Nd	72.00	51.60	25.90	44.50	17.00
Sm	14.20	13.30	6.12	6.02	3.20
Eu	1.26	1.39	0.47	1.37	0.74
Gd	12.10	14.60	6.84	4.78	2.44
Tb	1.99	2.60	1.24	0.55	0.39
Dy	11.70	16.10	8.60	2.68	2.29
Ho	2.39	3.29	1.85	0.39	0.48
Er	6.64	9.79	5.26	1.00	1.29
Tm	1.03	1.48	0.77	0.11	0.22
Yb	6.76	9.65	4.83	0.73	1.48
Lu	0.98	1.38	0.65	0.11	0.22
Zn	74.30	101.00	35.80	74.90	26.80
Ga	21.80	23.90	18.00	23.10	16.40
Cs	8.91	13.40	3.02	10.30	3.53
Rb	292.00	250.00	265.00	158.00	220.00
Sr	75.10	98.40	39.20	125.00	125.00
Ba	649.00	644.00	243.00	870.00	821.00
Zr	248.00	346.00	123.00	236.00	142.00
Nb	24.40	34.40	12.80	14.10	8.35
Ta	2.52	2.89	1.29	0.90	0.58
Hf	8.18	10.30	4.13	6.35	4.58
Th	33.20	24.40	19.70	10.60	19.30
U	6.62	6.74	5.32	1.70	1.88
Pb	37.50	26.80	26.80	17.40	37.00
V	17.00	28.10	6.24	25.40	12.70
Cr	4.57	7.33	2.91	11.80	2.86
Co	2.41	3.52	1.22	5.95	2.05
Ni	4.80	5.64	1.08	5.68	2.17
Cu	9.93	12.70	2.12	6.53	2.62
Eu*	0.29	0.30	0.72	0.78	0.81

Note: LOI—loss on ignition.

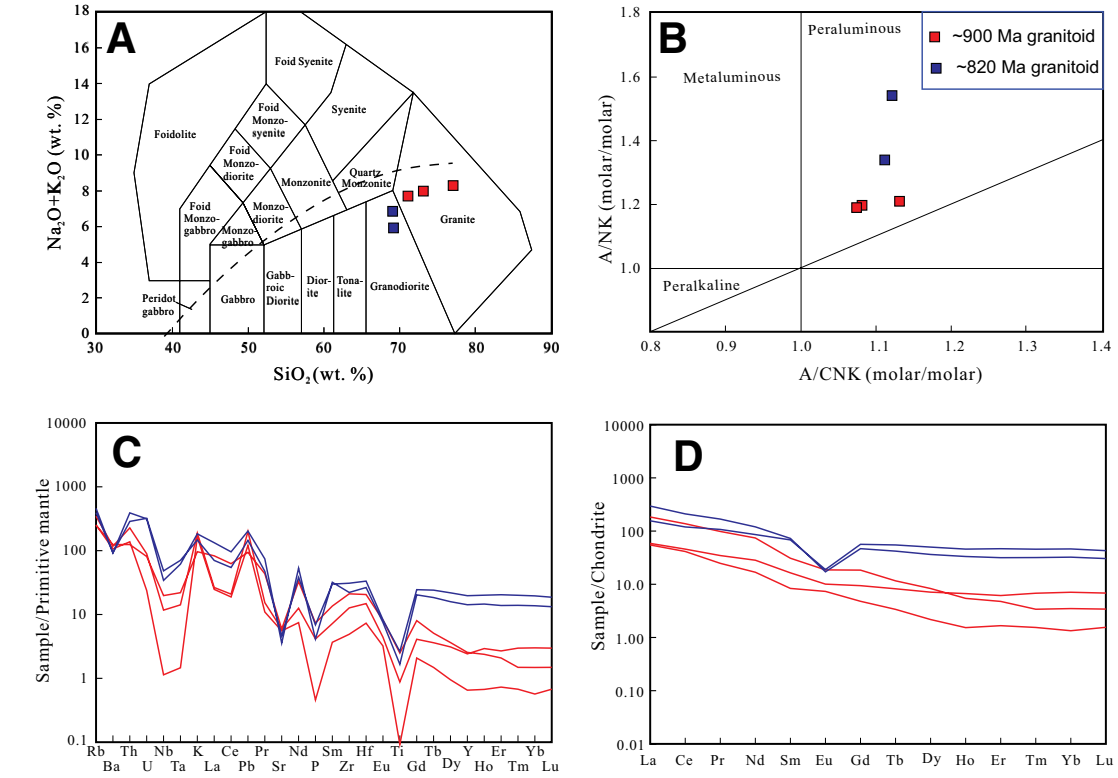

Figure 10. (A) SiO_2-(K_2O + Na_2O) (TAS, total alkali vs. silica) diagram for Proterozoic granitoids. Normalization values are from Middlemost (1994). (B) A/CNK versus A/NK diagram for Proterozoic granitoids. Normalization values are from Maniar and Piccoli (1989). (C) Primitive mantle-normalized trace element variation diagram for the analyzed Proterozoic granitoids. Normalization values are from Sun and McDonough (1989). (D) Chondrite-normalized rare earth element diagram for the analyzed Proterozoic granitoids. Normalization values are from Boynton (1984). (E) (10000 × Ga/Al)-Nb diagram for the analyzed Proterozoic granitoid samples. (F) (10000 × Ga/Al)-Zr diagram. Normalization values are from Pearce et al. (1984) and Pearce (1996). (G) Y versus Nb discrimination diagram for the analyzed Proterozoic granitoid samples. Normalization values are from Pearce et al. (1984). ORG—ocean ridge granites; VAG—volcanic arc granites; WPG—within plate granites; COLG—collision granites. (H) Yb + Ta versus Rb discrimination diagram. Normalization values are from Pearce et al. (1984).

diagram (Pearce et al., 1984; Pearce, 1996) the ca. 900 Ma plagiogneiss samples plot in the transition region between the volcanic arc–syncollisional and the within-plate fields, whereas the ca. 820 Ma metaporphyritic diorite samples are plot mostly in the within-plate field (Fig. 10H).

DISCUSSION

Ages, Geochemistry, and Tectonic Settings of the Neoproterozoic and Paleozoic Igneous Rocks

There are two populations of zircon ages observed in the Neoproterozoic granitoid samples: an early phase at ca. 900 Ma and a later phase at ca. 820 Ma. The early Paleozoic igneous samples yielded zircon ages of 472–468 Ma. All Neoproterozoic igneous samples belong to the peraluminous series (Fig. 10B). Discrimination diagrams suggest that the early ca. 900 Ma phase of granitoids was generated by arc magmatism and/or anatexis through crustal melting, whereas the younger ca. 820 Ma granitoids were generated during crustal extension (Figs. 10E, 10F). The geochemical differences between the ca. 900 Ma plagiogneiss samples and ca. 820 Ma metaporphyritic diorite samples are evident in the multielement diagrams, which show a much stronger depletion in Eu for the younger ca. 820 Ma samples (Figs. 10C, 10D). A compilation of all available ages of igneous rocks from the Qilian Shan region indicates similar age clusters at 960–880 Ma, 877–710 Ma, and 550–375 Ma (Fig. 11 and references cited therein).

Numerous 960–900 Ma granitoids have been reported across the Qilian Shan (Guo et al., 1999; Guo and Zhao, 2000; Gehrels et al., 2003b; Zhang et al., 2003; Tung et al., 2007; Song et al., 2012; Reith, 2013; Huang et al., 2015; Zuza, 2016) (Fig. 11). Some considered the 960–900 Ma gneisses to be the basement of the Qilian block (Tung et al., 2007), and our inherited zircon age data provide new evidence for the possible existence of Archean basement in the Qilian Shan region (Figs. 7 and 8). The 960–900 Ma magmatism has been related to the assembly of Rodina (Tseng et al., 2006; Song et al., 2010, 2013; He et al., 2012) or crustal anatexis (Chen et al., 2007). However, Huang et al. (2015) showed that this ca. 900 Ma magmatism involved a significant juvenile component, which contrasts the anatexis hypothesis.

The ca. 800 Ma granitoids are interpreted as reworked lower crustal melt that may have been induced by the underplating of mantle melt (Huang et al., 2015). Emplacement of granite and tonalite at ca. 775 Ma has been related to continental rifting, possibly of the Rodinian supercontinent (Tseng et al., 2006; Xu et al., 2015). Our ca. 820 Ma metaporphyritic diorite samples (WC2826 and WC2826–2 in Fig. 2) display geochemical characteristics of within-plate magmatism, consistent with the continental breakup hypothesis of Tseng et al. (2006; also see Lu et al., 2008; Tung et al., 2013).

Below, we outline our proposed history for the Proterozoic to early Paleozoic evolution of the Qilian region and its relationships to the neighboring North China craton, Tarim block, and the Qaidam-Kunlun terrane. The Qilian Ocean began opening in the Neoproterozoic, which coincided with the deposition of a tillite-bearing sequence in the Nanhua period (860–680 Ma) (Wang et al., 2013a; Xu et al., 2015). The reconstruction presented in Wu et al. (2016) assumed that the Qilian Ocean starting opening by ca. 750 Ma, but our new data regarding the ca. 820 Ma granitoid

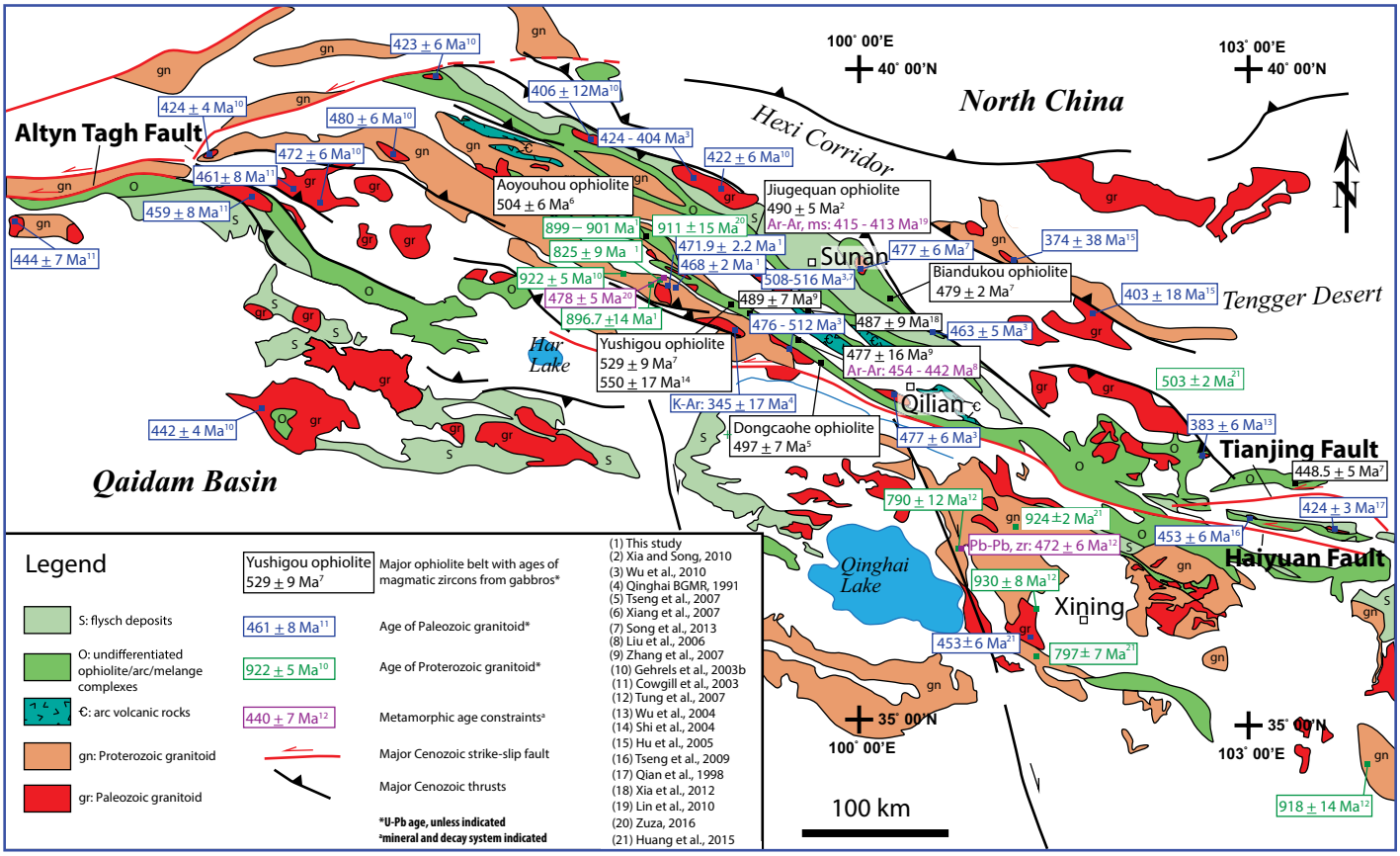

Figure 11. Simplified zircon U-Pb age distribution map showing magmatism across the Qilian Shan. S—Silurian; O—Ordovician; Є—Cambrian.

(sample WC2826) that is interpreted to be related to continental breakup suggests that rifting and ocean development may have occurred earlier.

There is no evidence of arc magmatism in the Qilian Shan from 710 to 550 Ma. Bimodal volcanism from ca. 775–600 Ma was associated with rifting, the continued development of the Qilian Ocean, and passive continental margin deposition (Tseng et al., 2006, 2007; Xu et al., 2015) (Fig. 12). The ocean-facing margins of the continents bounding the Qilian Ocean remained passive for at least 200 m.y., when the ocean reached its maximum extent in the Cambrian and subduction initiated along the northern margin of the Qaidam-Kunlun terrane (i.e., the southern boundary of the Qilian Ocean; Wu et al., 2016). Arc magmatism started at ca. 550–520 Ma within the Qaidaim-Kunlun terrane as a result of southward subduction of this ocean (Fig. 12). The mylonitic orthogneiss and plagioclase amphibolite samples, with ages of ca. 470 Ma, represent granitoid formation during the early-Middle Ordovician arc in the central Qilian Shan. The tectonic model of Huang et al. (2015) suggests that the ca. 450 Ma granitoids were generated in response to the closure of the Qilian Ocean and the onset of continental collision (Fig. 12). Consumption of the Qilian oceanic lithosphere may have continued until 400–375 Ma (Fig. 12), when igneous activities across the Qilian orogen ceased (see Wu et al., 2016, and references therein). However, some of these younger granitoids may have been generated by post–ocean closure crustal melting during protracted collisional orogeny (Fig. 12) (Gehrels et al., 2003b; Zhao et al., 2017).

Nature of the Central Qilian Basement

Detrital zircon ages record the crystallization age of an igneous source rock and/or a metamorphic overprinting, and thus can only place a maximum depositional age of the zircon-hosting strata. Our U-Pb detrital zircon dating provides valuable information about the provenance of the metasedimentary rocks in the central Qilian Shan. The quartzofeldspathic schist sample (WZ250413–5 in Fig. 2) collected from the Tuolai Group contained a single youngest zircon grain with a U-Pb age of ca. 1200 Ma, which defines the maximum depositional age of this schist sample (Fig. 9B). In addition, there are three prominent zircon populations with peaks at ca. 1440, ca. 1700, and ca. 2480 Ma. (Fig. 9B). The oldest zircon age is ca. 3090 Ma (Fig. 9B). Detrital zircon data from an additional Proterozoic (Pt_1) schist sample (AY 09–21–11[1]), which was collected from along the Tuo Lai River (Fig. 2), were presented in Zuza (2016). The sample has prominent age peaks at ca. 1430, ca. 1700, and ca. 1750 Ma, and minor Paleoproterozoic ages. The sample also has concordant Archean zircon grain ages (i.e., 2.52, 2.81, and 3.1 Ga; Zuza, 2016). The three youngest grains with overlapping ages have a weighted mean age of 1272 ± 20 Ma (MSWD = 1.8), consistent with our analysis of sample WZ250413–5, and this confirms a Mesoproterozoic age for the Pt_1 rock unit (Fig. 2). We suggest that the Tuolai Group was deposited between 1200 and 960 Ma based on our detrital zircon data and the intrusive relationships with early Neoproterozoic granitoids (Fig. 2) (Zuza et al., 2013).

Similar correlative Proterozoic units have been reported in northern Tibet. Gehrels et al. (2003a) presented detrital zircon ages from two Proterozoic samples, one in the central Qilian Shan (sample 5, GA206) and the other from the Altyn Tagh Range (sample 3, GA33) (Fig. 1A), which following the restoration of Cenozoic left-slip offset on the Altyn Tagh fault (e.g., Cowgill et al., 2003) aligns along strike with the Qilian Shan. These samples have ca. 1.2 and 1.60–1.45 Ga zircon populations and are both intruded by ca. 925 Ma granitoids (Gehrels et al., 2003a, 2003b). Detrital zircon ages from a Mesoproterozoic Dunzigou Group (e.g., Gong et al., 2013) quartzite sample from the Longshoushan (sample AZ 09–12–14 [2a]) in the southwestern North China craton also has a dominant ca. 1.5 Ga zircon population and ca. 1.2 Ga maximum depositional age (A.V. Zuza, personal data). In addition, unpublished age data for a quartzite sample from the Baiyinbaolage Formation of the Bayan Obo Group in the northern North China craton shows two prominent zircon age populations at 1740–1580 and 1300–1200 Ma (Z. Zhou, personal data). The youngest and oldest zircon ages are ca. 1247 and ca. 2962 Ma, respectively.

These samples from the Mesoproterozoic Qilian strata, including the Tuolai Group of this study, and North China craton have numerous similarities, including ca. 1.2 Ga youngest zircon grain ages, Archean zircon grains, and a pronounced ca. 1.5 Ga zircon age signature (Fig. 13), which is not common in Asia (see Demoux et al., 2009; Rojas-Agramonte et

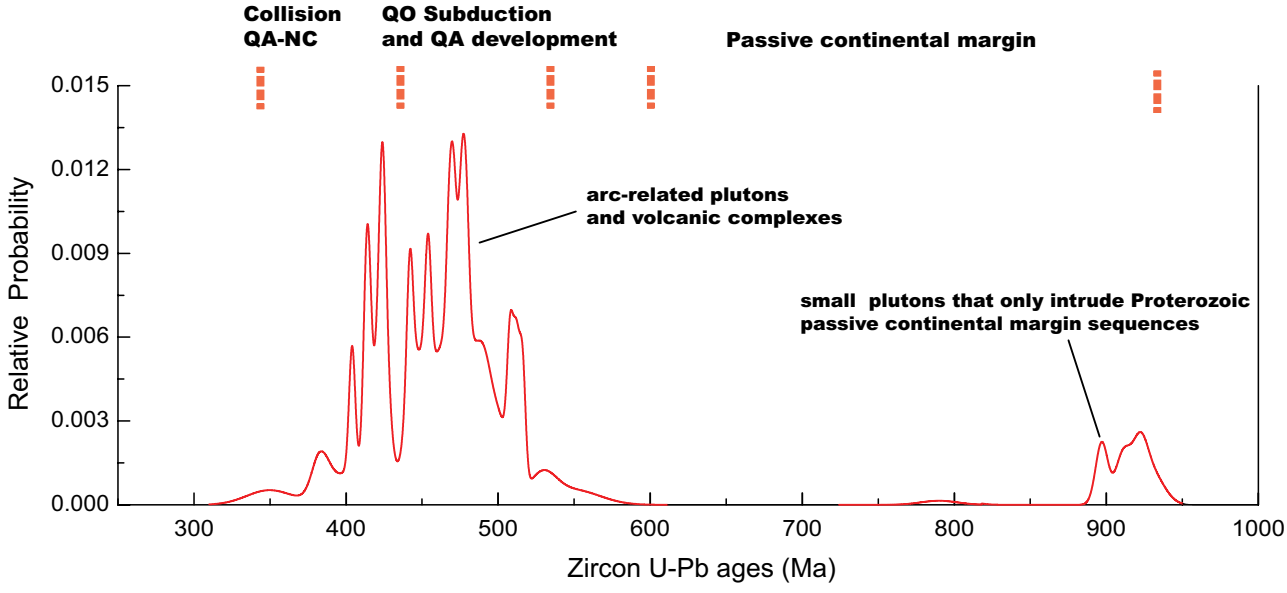

Figure 12. Probability distribution plot of all U-Pb ages across the Qilian Shan in the northern Tibet. The number of data points is 72; see Figure 10 for details. QO—Qilian Ocean; QA–Qilian arc; NC–North China craton.

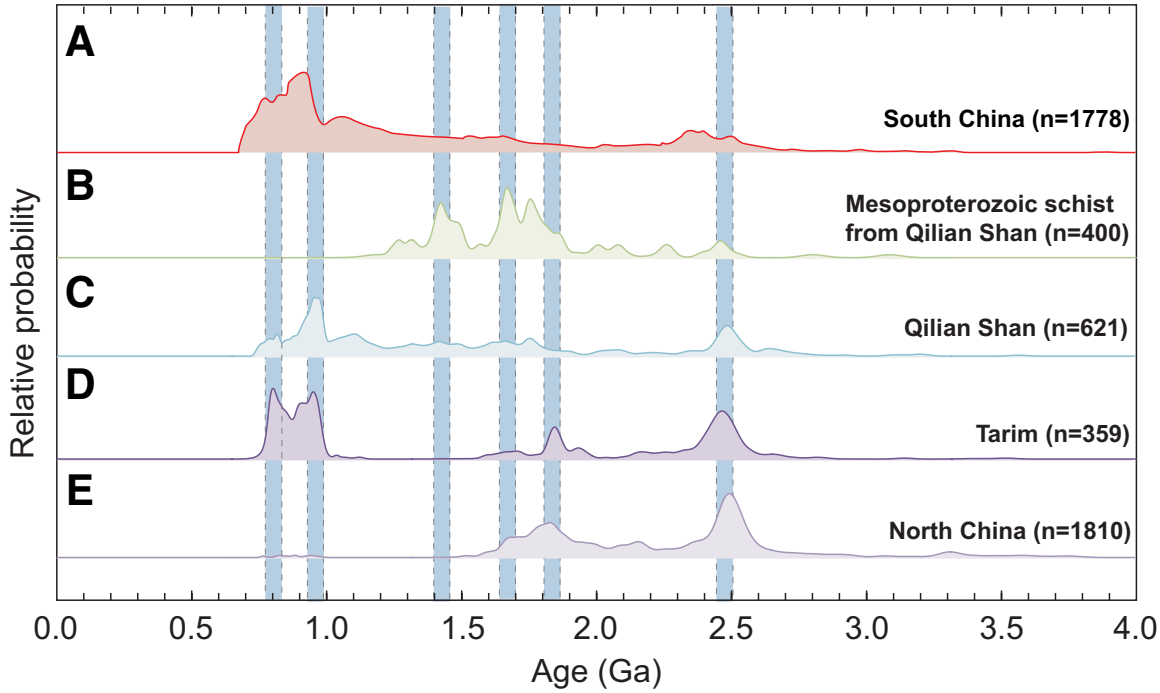

Figure 13. Normalized probability plot of zircon ages older than 750 Ma. (A) From the South China craton. (B, C) From the Qilian Shan. (D) From the Tarim craton. (E) From the North China craton. U-Pb ages were used for zircons younger than 1000 Ma and Pb-Pb ages were used for older zircons. Blue shaded zones denote prominent age peaks at ca. 760–820 Ma, 960–890 Ma, 1450–1400 Ma, 1700–1650 Ma, 1850–1800 Ma, and 2500–2450 Ma, which correspond to widespread tectonic events as discussed in the text. South China ages from Zhao and Cawood (2012), Cawood et al. (2013) and Xu et al. (2014). The Qilian Shan data are a compilation of our own work and Zuza (2016). Tarim and North China craton data were compiled by Rojas-Agramonte et al. (2011).

al., 2011; C.F. Liu, personal data). We therefore propose that these rocks with a common relatively distinct zircon-age signature were part of a single regionally extensive unit that extended from the Altyn Tagh Range (western Qilian Shan) to the North China craton. For this correlation to be valid there must be suitable protolith rocks to provide the observed ca. 1.5 Ga zircon age signature. One possibility is that 1.52 Ga gneiss from the Baga Bogd massif (Demoux et al., 2009), which is one of the Central Asia microcontinents within the Central Asian Orogenic System, provided such a source (Fig. 1A). This gneiss was intruded by ca. 950 Ma granites (Demoux et al., 2009) and it has been argued that this microcontinent originated from the northern margin (present-day coordinates) of a linked Tarim–North China continent that later drifted into the Paleo–Asian Ocean in the early Neoproterozoic (e.g., Rojas-Agramonte et al., 2011; Zuza and Yin, 2014). The restored Mesoproterozoic position of this localized ca. 1.5 Ga source in the Tarim–North China craton could have provided detritus that was deposited in this regionally extensive unit. This implies that the Qilian basement rocks were once part of the North China craton, although additional future analyses are required to confirm this hypothesis.

Mesoproterozoic strata in the central Qilian Shan contain Paleoproterozoic and Archean zircon grains, which have been largely ignored in the existing literature (Figs. 13B, 13C). Our early Paleozoic plagioclase-amphibolite sample (WC2821) also contains inherited Neoarchean–Paleoproterozoic zircons with ages of 2020, 2060, and 2660 Ma (Fig. 7). The inherited zircon grains older than 1.0 Ga define an Archean concordia intercept age of ca. 2700 Ma, and a similar age is observed in individual inherited zircons from the amphibolite and eclogite samples (WC2821 and WC4173) (for individual zircon-grain ages see Table DR1). These ages confirm the existence of Archean basement in the central Qilian Shan. Furthermore, Proterozoic metasedimentary samples from the Qilian Shan shows three prominent zircon age peaks at ca. 1430, ca. 1700, and ca. 2480 Ma (Fig. 13B) (data compiled from Zuza, 2016; C.F. Liu, personal data; and this study). Detrital zircon ages from a Proterozoic continental quartzite sample in the Tuolai Group with age clusters at 1.3–1.2 and 2.0–1.7 Ga, and minor peaks at ca. 2.7 and ca. 2.2 Ga, were reported in Zuza (2016), which suggests that there was Archean basement in the source region for these metasedimentary rocks.

The most important period of crustal growth in the North China craton was at ca. 2.5 Ga (Fig. 13E) (e.g., Kusky et al., 2007, 2016; Wan et al., 2015). North China Archean–Paleoproterozoic rocks are overlain by the 1.85–1.40 Ga strata as part of the Mesoproterozoic Changcheng (Great Wall)-Jixian systems (Kusky et al., 2007; Chinese Geological Survey, 2014). There is some consensus that most of these rocks were deposited during postorogenic extension, and 1800–1700 Ma zircon grains are the most dominant (Fig. 13E) (e.g., Liu et al., 2006; Kusky et al., 2007). Magmatism at 1400–1240 Ma in the northern North China craton includes a ca. 1400 Ma carbonatite dike (Fan et al., 2014), ca. 1342 Ma gabbro (Zhou et al., 2016), and 1247–1350 Ma granitoids (Zhang et al., 2009, 2012). These intrusions could be the sources for the ca. 1.2 and 1.4 Ga zircon grains in the Proterozoic Tuolai Group and correlated strata (e.g., Fig. 9B) (Gehrels et al., 2003a; this study).

The pre-Neoproterozoic Qilian basement rocks are intruded by widespread 1.0–0.8 Ga granitoids (Fig. 11) (Guo et al., 1999; Guo and Zhao, 2000; Gehrels et al., 2003b; Zhang et al., 2003; Tung et al., 2007; Song et al., 2012; Reith, 2013; Huang et al., 2015; Zuza, 2016; this study). These

intrusions are sometimes referred to as Grenvillian in age (ca. 1.3–0.9 Ga) (e.g., Ma et al., 2012; Kröner et al., 2013a, 2013b; He et al., 2014) and are correlated with other Grenvillian basement rocks, including the Yangtze block of southern China (Fig. 13) or other Gondwana continents (e.g., Wan et al., 2001; Tung et al., 2007, 2013; Lu et al., 2008, 2009; Song et al., 2013; Xu et al., 2015). However, we note that this 400 m.y. time period is not particularly useful for correlating continents, and zircon signatures of this age are found in East Antarctica, India, Australia, Central Asia, southern China, and Tarim (e.g., Fitzsimons, 2000; Peng et al., 2011a, 2011b; Chattopadhyay et al., 2015). Due to this non-uniqueness, we only focus on the geochemically and geologically derived tectonic setting and context of these 1.0–0.8 Ga intrusions.

Wan et al. (2001) suggested that the 1.0–0.8 Ga granitic rocks were the product of continent-continent collision, possibly related to widespread Neoproterozoic collisions during the construction of the supercontinent Rodinia (e.g., Fitzsimons, 2000; Li et al., 2002; Z.X. Li et al., 2008; He et al., 2012). Based on our geochemical analysis (Fig. 10), we suggest that the distinct ca. 900 and ca. 820 Ma age populations represent arc magmatism during with crustal growth (ca. 900 Ma) followed by crustal reworking via extensional processes (ca. 820 Ma). Whole rock Sr-Nd-Pb-Hf isotopic analyses by Huang et al. (2015) support these tectonic settings. The Mesoproterozoic Tuolai Group and equivalent strata in northern China and the Altyn Tagh Range (Gehrels et al., 2003a; this study) were intruded by similar ca. 0.95–0.9 Ga granitoid rocks; this leads us to suggest that arc magmatism at ca. 900 Ma affected the southern margin of a contiguous Tarim–North China craton that included the Qilian basement.

As discussed here, the North Tarim–North China and the South Tarim–Qaidam–Kunlun terranes had coalesced by ca. 850 Ma, and this linked continent started rifting by 820–775 Ma with the opening of the Qilian Ocean. North China and the Qaidam-Kunlune terrane separated, and passive margin sediments were deposited on the ocean-facing margins of each continent. Late Neoproterozoic passive margin sediments (i.e., marbles and schist interbedded with basalt) are exposed throughout the central Qilian Shan (Fig. 2); the local passive margin strata (e.g., Zhulongguan Group) were recently described by Xu et al. (2015). Here we argue based on field relationships that these late Neoproterozoic passive margin sediments, which included interbedded ca. 600 Ma basalt (Xu et al., 2015), are actually part of the North China craton's southern margin, not the Qaidam-Kunlun terrane's northern margin (present-day coordinates). It is important to note that late Neoproterozoic marbles and schist rocks in the central Qilian Shan (Fig. 2) are not intruded by Ordovician Qilian arc granitoids, as would be expected for Qaidam-Kunlun's passive margin strata on which the south-dipping Qilian arc was constructed (Gehrels et al., 2003a, 2003b; Yin et al., 2007a). Instead we suggest that these late Neoproterozoic passive margin strata, originally deposited on the North China craton, were underthrust beneath the Qaidam-Kunlun terrane and/or exhumed north of the arc in a foreland thrust system (e.g., the Tethyan strata in the Himalaya) during the early Paleozoic Qilian orogen. The first scenario is supported by the observation that these passive margin sediments are always in tectonic contact with the Cambrian ophiolitic mélange unit (e.g., Xu et al., 2015; Zuza, 2016). This interpretation suggests that these Zhulongguan Group rocks correlate with the Neoproterozoic Hanmushan Group in the Longshoushan (Li, 1991). The only detrital zircon analyses of Neoproterozoic strata in the Qilian Shan that we are aware of are from the westernmost Qilian Shan (sample 4, GA209) (Gehrels et al., 2003a). This sample has 0.9, 1.2, and 1.5 Ga zircon age populations (Gehrels et al., 2003a), which correlate with zircon peaks from the Mesoproterozoic Tuolai Group (Fig. 13).

Southward subduction during Qilian arc was responsible for bringing the observed eclogite samples to UHP depths beneath the Qaidam-Kunlun terrane (e.g., Gehrels et al., 2003b; Yin et al., 2007a; Wu et al., 2016; Menold et al., 2016). Diverse Archean–Proterozoic zircon ages from eclogite sample WC4173 (Fig. 9) require either a sedimentary rock protolith for the eclogite or that the mafic-igneous protolith intruded through Archean–Proterozoic basement. The pronounced ca. 916 Ma zircon age peak and Archean–Proterozoic grains suggest that this protolith was originally Qaidam-Kunlun basement, which is similar to North China basement with Archean–Proterozoic zircons. Taken together, these observations support our proposal that the Qilian basement has a close affinity to the North China craton (Fig. 13E), as opposed to the South China craton (Fig. 13A).

In summary, although data regarding the Qilian basement is still reconnaissance in nature, the available field relationships and detrital zircon ages suggest the following. (1) Regionally extensive Mesoproterozoic strata (e.g., the Tuolai Group) were deposited on the southern margin of the Tarim–North China continent, and the detrital zircon signature in these sediments has significant ca. 1.2 and 1.4–1.5 Ga peaks. (2) Mesoproterozoic supracrustal rocks of the southern Tarim–North China margin were intruded by 1.0–0.9 Ga arc-related intrusions, as evidenced by intrusions in Tarim, the Atlyn Tagh Range, the Qilian Shan, and northern China. (3) Late Neoproterozoic rifting was followed by passive margin development along the southern margin of the North China craton, the development of the Qilian Ocean, and the separation of the Tarim–North China continent from the Qaidam-Kunlun terrane. (4) South-dipping subduction beneath the Qaidam-Kunlun terrane in the early Paleozoic Qilian arc resulted in the southward underthrusting of the southern margin of the North China craton beneath the Qaidam-Kunlun terrane. This led to the tectonic mingling of the North China craton Neoproterozoic passive margin (i.e., the Zhulongguan and Hanmushan Groups), eclogite lenses derived from an Archean–Proterozoic basement source, and the Qaidam-Kunlun terrane.

Mesoproterozoic–Early Paleozoic Tectonic Evolution of Northern Tibet

Based on the data presented here and other regional studies, we propose the following tectonic model for the Mesoproterozoic to early Paleozoic geologic history of northern Tibet (Fig. 14). In the Mesoproterozoic, a combined Tarim–North China continent was bound to the south by the Paleo–Qilian Ocean (Fig. 14A). Passive margin sedimentation along the southern continental margin included ca. 2.7, ca. 1.8, and 1.5–1.4 Ga zircon grains likely derived from the North China craton, as supported by the detrital zircon data in Gehrels et al. (2003a), Zuza (2016), and this study (i.e., the Tuolai Group schist sample; Fig. 9B). Note that the Bayan Obo Group, which contains similar zircon ages, was likely deposited at a similar time along the northern North China craton margin, although this is outside the scope of this study (Fig. 14A). The 1.0–0.89 Ga granitoid plutons intruded the southern passive margin strata during the development of a continental arc that accommodated the eventual closure of the Paleo–Qilian Ocean (e.g., Wu et al., 2016) (Fig. 14B). Although the polarity of this subduction zone is poorly constrained, the South Tarim and Qaidam-Kunlun continents lack plutonic rocks of this age, and thus we infer that the closure of the Paleo–Qilian Ocean was accomplished by a north-dipping subduction zone. The ca. 820 Ma within-plate A-type granites reported herein may have resulted from postorogenic extension (Fig. 10), which indicates that final closure of the Paleo–Qilian Ocean should have occurred after ca. 900 Ma but before ca. 820 Ma. We assume an ocean-closure age of ca. 850 Ma in our reconstruction (Fig. 14C).

Late Neoproterozoic rifting of this linked continent led to the opening of the Qilian Ocean to the south and the Paleo–Asian Ocean (Fig. 14D). The lack of observed Phanerozoic sutures or amalgamation structures

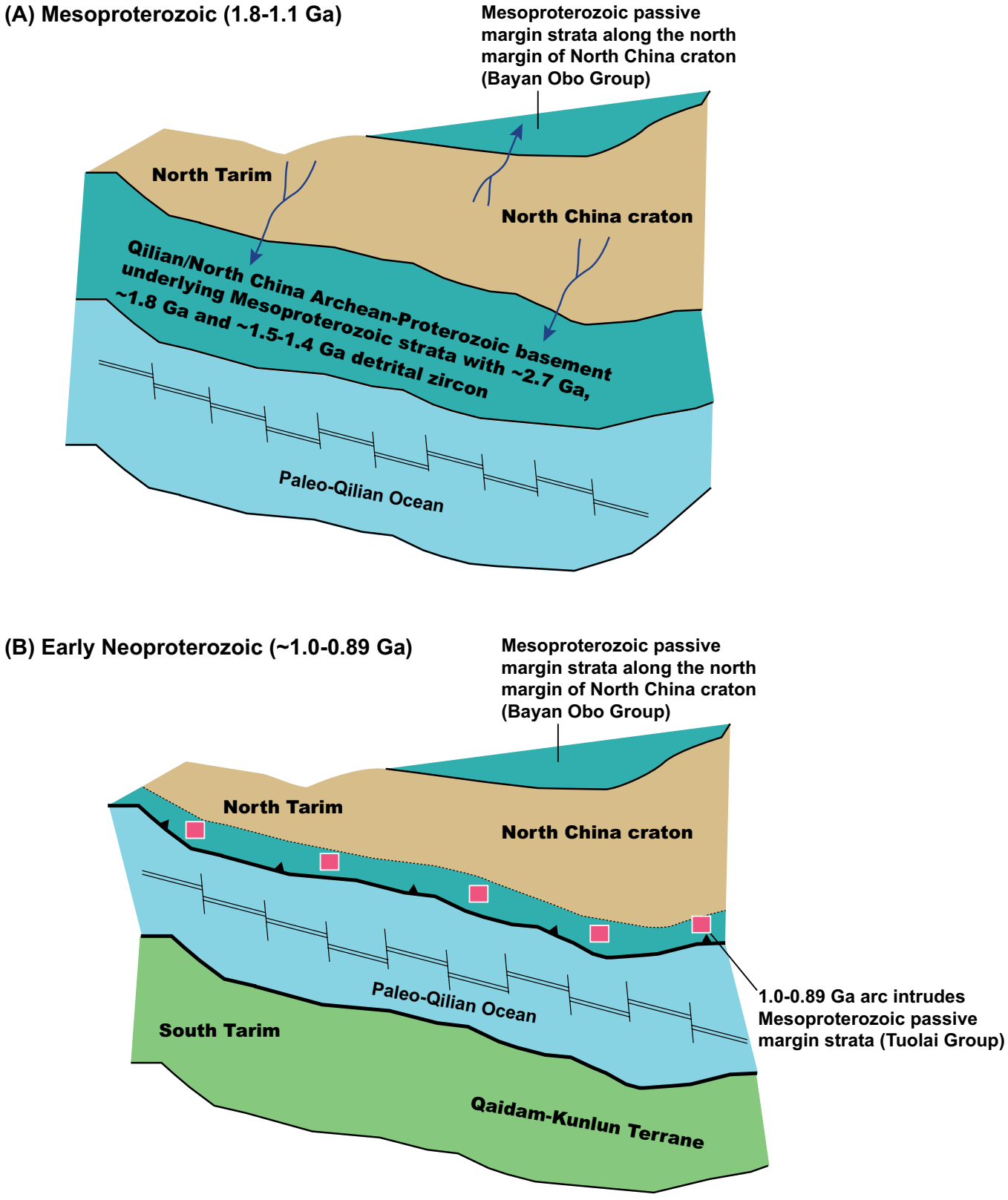

Figure 14. Models for the tectonic evolution of northern Tibet and the Qilian Shan from the Mesoproterozoic through the Silurian. Note that the scale is relative and changes. (A) In the Mesoproterozoic, cratonal and/or passive margin deposits along the southern margin of a combined North Tarim–North China continent contain ca. 2.7, ca. 1.8 and ca. 1.4 Ga detrital zircon grains. (B) Early Neoproterozoic north-dipping subduction leads to the development of the Paleo–Qilian arc (with ca. 1.0–0.89 Ga magmatism), which accommodates convergence between the South Tarim–Qaidam–Kunlun and North Tarim–North China continents. (*Continued on following two pages.*)

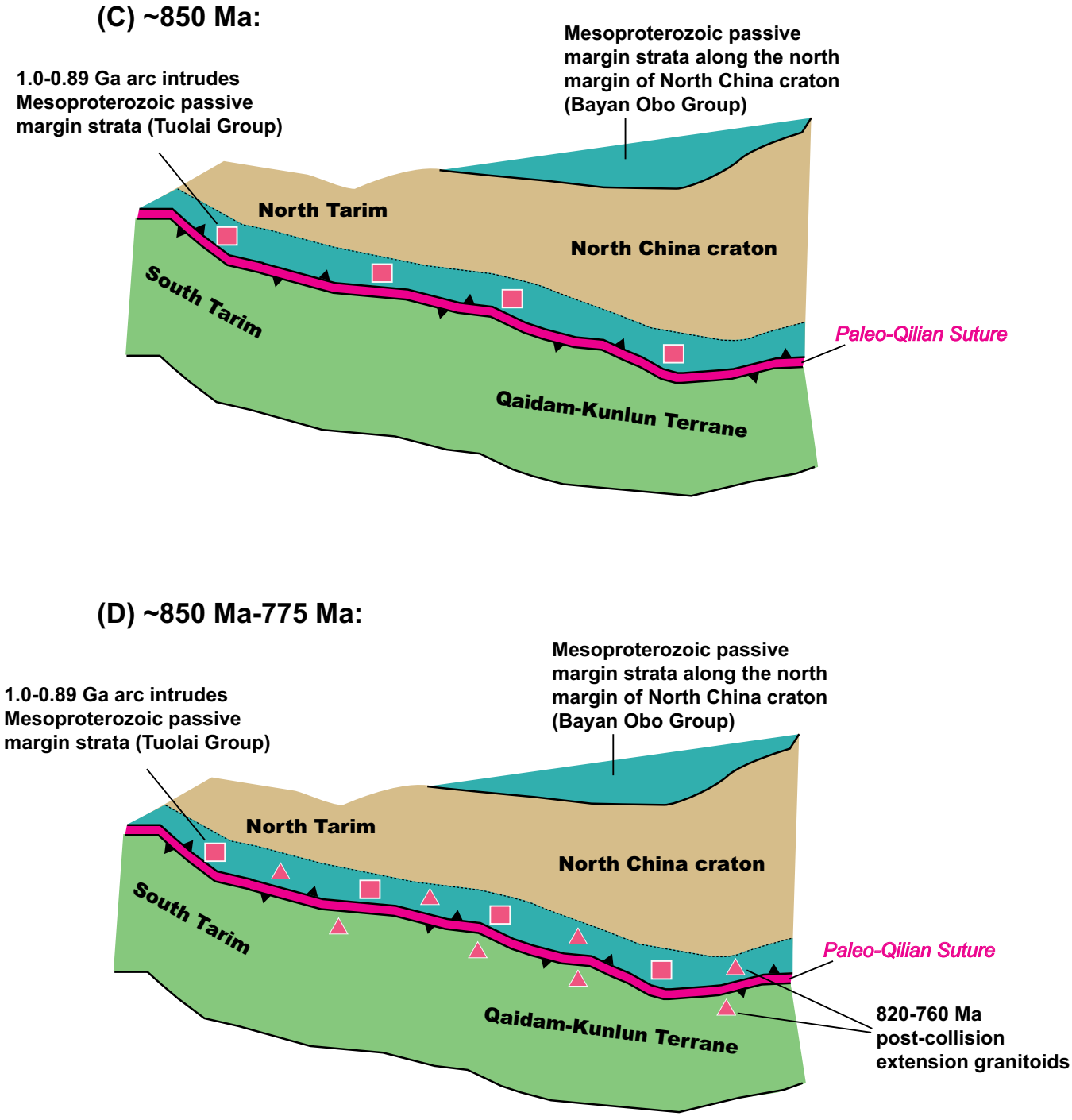

Figure 14 (*continued*). (C) North-dipping subduction leads to the closure of the Paleo–Qilian Ocean by ca. 830 Ma. (D) Late Neoproterozoic rifting leads to the opening of the Qilian and Paleo–Asian Oceans. Bimodal volcanism (ca. 830–600 Ma) occurs throughout the Qaidam-Kunlun, Tarim, and North China cratons. (*Continued on following page.*)

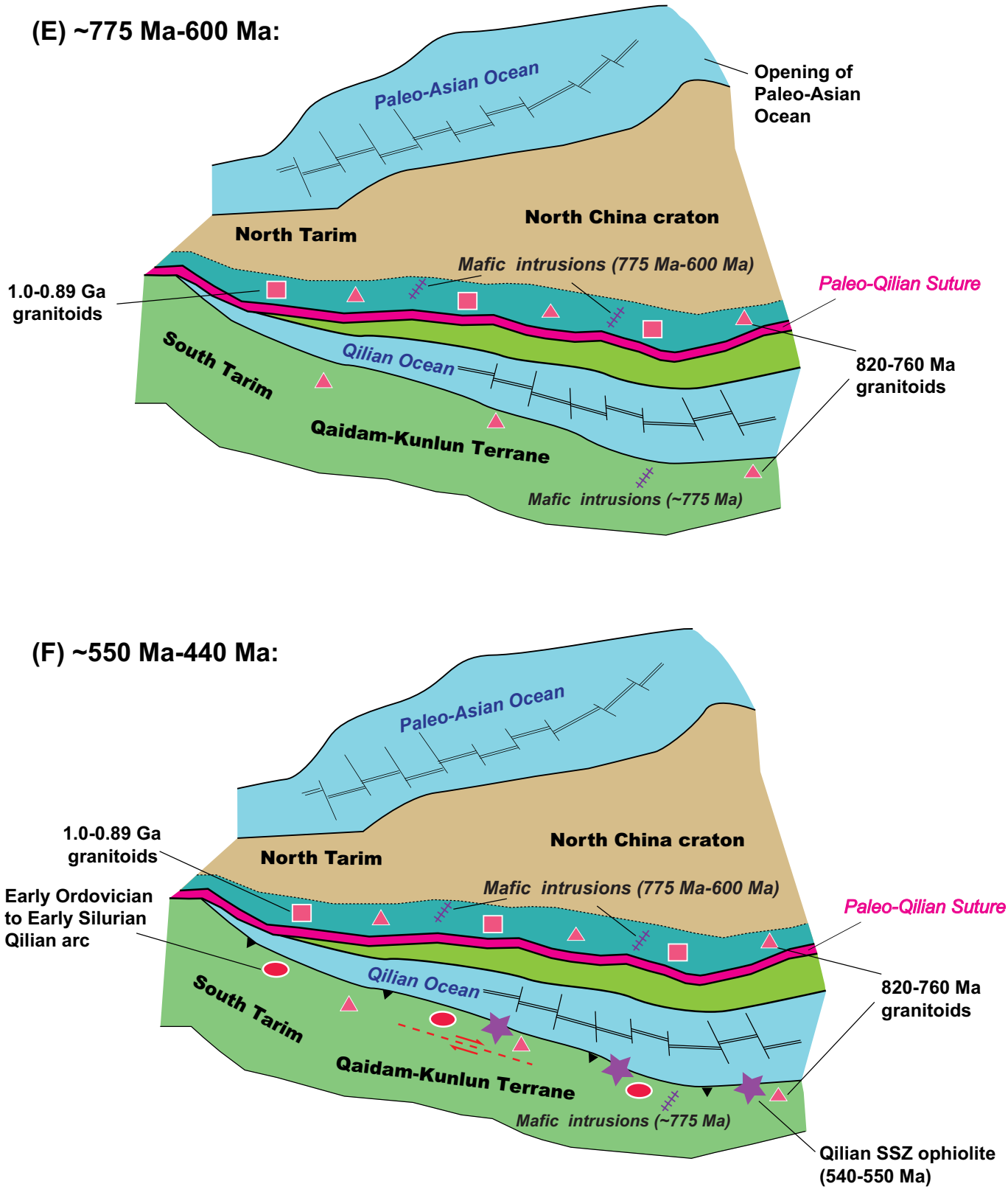

Figure 14 (*continued*). (E) Cambrian suprasubduction zone (SSZ) ophiolites (ca. 540–500 Ma) are generated in an incipient arc setting as south-dipping subduction begins just north of the Qaidam-Kunlun northern margin. Continental arc magmatism begins in the Ordovician, along with a trench-parallel intra-arc right-lateral strike-slip fault. Continental crust is brought to ultrahigh-pressure depths along the subduction channel. (F) Collision between the Qaidam-Kunlun continent and North China craton occurs at ca. 445–440 Ma and is associated with a magmatic pulse at that time. Synorogenic and postorogenic magmatism is diffuse but widespread.

between the South Tarim and Qaidam continents suggests that they were connected prior to and during the opening of the Qilian Ocean (e.g., Zuza, 2016). Bimodal volcanism from ca. 775 to 600 Ma and passive margin deposition across the Qaidam-Kunlun terrane and North China craton (Tseng et al., 2006, 2007; Xu et al., 2015; Wu et al., 2016) was associated with the opening of the Qilian Ocean. Cambrian suprasubduction zone ophiolites (ca. 540–500 Ma) (e.g., Yang et al., 2002; Shi et al., 2004; Tseng et al., 2007; Xia and Song, 2010; Lin et al., 2010; Song et al., 2013) developed along the northern edge of the Qaidam-Kunlun terrane and are evidence for the initiation of southward subduction of the Qilian Ocean (Fig. 14E). Continued Ordovician subduction and arc magmatism led to the convergence of the Tarim–North China craton and Qaidam-Kunlun terrane. Collision between these continents may have occurred in the latest Ordovician to earliest Silurian (ca. 445–440 Ma) (Fig. 14F). A ca. 442 Ma syncollisional granite in North Qaidam was documented in Zhang et al. (2017), and Yang et al. (2016) suggested that the Late Ordovician to middle Silurian granitoids developed in a postcollision setting. In addition, a single young zircon from our mylonitic orthogneiss sample shows an age of 445 Ma (Fig. 8E), and a peak of monazite ages corresponding to this time period was reported in Zuza (2016).

CONCLUSIONS

Our work establishes, through geologic mapping and U-Pb zircon geochronology, the structural framework of an ~1500 km^2 region in the central Qilian Shan. This study identified the Cenozoic Shule and Tuolai thrust systems. We present laser ablation–inductively coupled plasma–mass spectrometry U-Pb zircon ages of samples collected from these thrust systems that record Neoproterozoic to Paleozoic granitoids. Our U-Pb zircon dating indicates that the Qilian basement underwent at least three periods of magmatism since the Neoproterozoic: (1) 960–880 Ma, (2) 877–710 Ma, and (3) 550–375 Ma. Zircons from high-pressure and UHP eclogites from the north-central Qilian Shan suggest that the igneous protolith has an age of ca. 916 Ma. Most zircons display recrystallized rims, and our dating of these rims suggests that eclogite facies metamorphism occurred at ca. 485 Ma. Our detrital zircon ages for the Proterozoic Tuolai Group indicate that it was deposited between 1203 and 960 Ma, and correlation with other Mesoproterozoic units across northern Tibet suggest these rocks were deposited in a regionally extensive basin along the southern margin of the North China craton.

We integrate our U-Pb zircon ages with stratigraphic data to discuss the origin and tectonic evolution of the Precambrian basement of the central Qilian Shan, and provide further support for the hypothesis that the central Qilian basement was originally part of the North China craton. The magmatic history, together with the geologic constraints obtained from this study and existing work in the neighboring regions, allows us to construct a coherent tectonic model that explains the evolution of the northern Tibet from the Mesoproterozoic to the early Paleozoic. Our model has the following key features. (1) The Paleo–Qilian Ocean existed between the linked North Tarim–North China craton and the South Tarim–Qaidam–Kunlun terranes in the early Mesoproterozoic. (2) This ocean closed via the collision of these two continents after ca. 900 Ma but before ca. 820 Ma. (3) The Qilian Ocean opened in the late Neoproterozoic as a small marginal sea along the southern margin of the Laurasian continent, not as a throughgoing ocean separating Gondwana from Laurasia. (4) South-dipping subduction of the Qilian Ocean beneath the Qaidam-Kunlun terrane led to the development of the Qilian arc and accommodated final closure of the ocean during the collision between the Tarim–North China craton and the Qaidam-Kunlun terrane in the Late Ordovician–early Silurian (445–440 Ma).

ACKNOWLEDGMENTS

We thank Junfeng Gong, Hongyuan Zhang, Ke Huang, and Long Wu for assistance in the field. Constructive reviews by three anonymous reviewers led to significant improvements of the original manuscript. This work was supported by the China University of Geosciences (Beijing) and a grant from the SinoProbe Program administered by the Chinese Academy of Geological Sciences (SinoProbe-08–01) and the Qilian Mapping Program administered by the Institute of Geological Survey (project 1212011121188), China University of Geosciences (Beijing).

REFERENCES CITED

Andersen, T., 2002, Correction of common lead in U-Pb analyses that do not report ^{204}Pb: Chemical Geology, v. 192, p. 59–79, doi:10.1016/S0009-2541(02)00195-X.

Boynton, W.V., 1984, Cosmochemistry of the rare earth elements: Meteorite studies, *in* Henderson, P., ed., Rare Earth Element Geochemistry: Amsterdam, Netherlands, Elsevier, p. 63–114, doi:10.1016/B978-0-444-42148-7.50008-3.

Cawood, P.A., Wang, Y.J., Xu, Y.J., and Zhao, G.C., 2013, Locating south China in Rodinia and Gondwana: A fragment of greater India lithosphere?: Geology, v. 41, p. 903–906, doi:10.1130/G34395.1.

Chattopadhyay, S., Upadhyay, D., Nanda, J.K., Mezger, K., Pruseth, K.L., and Berndt, J., 2015, Proto-India was a part of Rodinia: Evidence from Grenville-age suturing of the Eastern Ghats Province with the Paleoarchean Singhbhum Craton: Precambrian Research, v. 266, p. 506–529, doi:10.1016/j.precamres.2015.05.030.

Chen, N.S., Xia, X.P., Li, X.Y., and Sun, M., 2007, Timing of magmatism of the gneissic-granite plutons along north Qaidam margin and implications for Precambrian crustal accretions: Zircon U-Pb dating and Hf isotope evidences: Yanshi Xuebao, v. 23, p. 501–512 (in Chinese with English abstract).

Chen, X.H., Yin, A., Gehrels, G.E., Cowgill, E.S., Grove, M., Harrison, T.M., and Wang, X.-F., 2003, Two phases of Mesozoic north-south extension in the eastern Altyn Tagh range, northern Tibetan Plateau: Tectonics, v. 22, 1053, doi:10.1029/2001TC001336.

Chen, Y., Xu, B., Zhan, S., and Li, Y., 2004, First mid-Neoproterozoic paleomagnetic results from the Tarim Basin (NW China) and their geodynamic implications: Precambrian Research, v. 133, p. 271–281, doi:10.1016/j.precamres.2004.05.002.

Chinese Geological Survey, 2014, Geologic time units in China: Beijing, Geological Publishing House.

Clark, M.K., and Royden, L.H., 2000, Topographic ooze: Building the eastern margin of Tibet by lower crustal flow: Geology, v. 28, p. 703–706, doi:10.1130/0091-7613(2000)28<703:TOBTEM>2.0.CO;2.

Cowgill, E., Yin, A., Harrison, T.M., and Wang, X.F., 2003, Reconstruction of the Altyn Tagh fault based on U-Pb geochronology: Role of back thrusts, mantle sutures, and heterogeneous crustal strength in forming the Tibetan Plateau. Journal of Geophysical Research, v. 108, 2346, doi:10.1029/2002JB002080.

Dan, W., Li, X.H., Guo, J., Liu, Y., and Wang, X.C., 2012, Paleoproterozoic evolution of the eastern Alxa Block, westernmost North China: Evidence from in situ zircon U-Pb dating and Hf-O isotopes: Gondwana Research, v. 21, p. 838–864, doi:10.1016/j.gr.2011.09.004.

Demoux, A., Kröner, A., Badarch, G., Jian, P., Tomurhuu, D., and Wingate, M.T., 2009, Zircon ages from the Baydrag block and the Bayankhongor ophiolite zone: Time constraints on late Neoproterozoic to Cambrian subduction-and accretion-related magmatism in central Mongolia: Journal of Geology, v. 117, p. 377–397, doi:10.1086/598947.

Ding, L., Yang, D., Cai, F.L., Pullen, A., Kapp, P., Gehrels, G.E., Zhang, L.Y., Zhang, Q.H., Lai, Q.Z., Yue, Y.H., and Shi, R.D., 2013, Provenance analysis of the Mesozoic Hoh-Xil-Songpan-Ganzi turbidites in northern Tibet: Implications for the tectonic evolution of the eastern Paleo-Tethys Ocean: Tectonics, v. 32, p. 34–48, doi:10.1002/tect.20013.

Dong, Y.P., and Santosh, M., 2015, Tectonic architecture and multiple orogeny of the Qinling orogenic belt, Central China: Gondwana Research, v. 29, p. 1–40, doi:10.1016 /j.gr.2015.06.009.

Du, Y., Wang, J., Han, X., and Shi, G.R., 2003, From flysch to molasse—Sedimentary and tectonic evolution of late Caledonian–early Hercynian foreland basin in North Qilian Mountains: Journal of China University of Geosciences, v. 14, p. 1–7.

Eby, G.N., 1990, The A-type granitoids: A review 1178 of their occurrence and chemical characteristics and speculations on their petrogenesis: Lithos, v. 26, p. 115–134, doi:10.1016 /0024-4937(90)90043-Z.

Eby, G.N., 1992, Chemical subdivision of the A-type granitoids: petrogenetic and tectonic implications: Geology, v. 20, p. 641–644, doi:10.1130/0091-7613(1992)020<0641:CSOTAT>2.3.CO;2.

Fan, H.R., Ha, F.F., Yang, K.F., Pirajno, F., Liu, X., and Wang, K.Y., 2014, Integrated U-Pb and Sm-Nd geochronology for a REE-rich carbonatite dyke at the giant Bayan Obo REE deposit, northern China: Ore Geology Reviews, v. 63, p. 510–519, doi:10.1016/j.oregeorev.2014.03.005.

Faure, M., Trap, P., Lin, W., Monié, P., and Bruguier, O., 2007, Polyorogenic evolution of the Paleoproterozoic Trans-North China Belt, new insights from the Lüliangshan-Hengshan-Wutaishan and Fuping massifs: Episodes, v. 30, p. 95–106.

Feng, Y., and He, S., 1996, Tectonics and orogeny of Qilian mountains: Beijing, Geological Publishing House, 238 p. (in Chinese with English abstract).

Fitzsimons, I.C.W., 2000, Grenville-age basement provinces in East Antarctica: Evidence for three separate collisional orogens: Geology, v. 28, p. 879–882, doi:10.1130/0091-7613(2000)28<879:GBPIEA>2.0.CO;2.

Gansu Geological Bureau, 1989, Regional geology of Gansu Province: Beijing, Geological Publishing House, 692 p. (in Chinese).

Gao, Z.J., Chen, J.B., Lu, S.N., Peng, C.W., and Qin, Z.Y., 1993, The Precambrian geology in northern Xinjiang: Precambrian Geology, v. 6, 171 p. (in Chinese).

Gao, R., Wang, H., Yin, A., Dong, S., Kuang, Z., Zuza, A.V., Li, W., and Xiong, X., 2013, Tectonic development of the northeastern Tibetan Plateau as constrained by high-resolution deep seismic-reflection data: Lithosphere, v. 5, p. 555–574, doi:10.1130/L293.1.

Ge, R., Zhu, W., Wilde, S.A., He, J., and Cui, X., 2015, Synchronous crustal growth and reworking recorded in late Paleoproterozoic granitoids in the northern Tarim craton: In situ zircon U-Pb-Hf-O isotopic and geochemical constraints and tectonic implications: Geological Society of America Bulletin, v. 127, p. 781–803, doi:10.1130/B31050.1.

Ge, R., Zhu, W., and Wilde, S.A., 2016, Mid-Neoproterozoic (ca. 830–800 Ma) metamorphic P-T paths link Tarim to the circum-Rodinia subduction-accretion system: Tectonics, v. 35, p. 1465–1488, doi:10.1002/2016TC004177.

Gehrels, G.E., Yin, A., and Wang, X.F., 2003a, Detrital-zircon geochronology of the northeastern Tibetan plateau: Geological Society of America Bulletin, v. 115, p. 881–896, doi:10.1130/0016-7606(2003)115<0881:DGOTNT>2.0.CO;2.

Gehrels, G.E., Yin, A., and Wang, X.F., 2003b, Magmatic history of the northeastern Tibetan Plateau: Journal of Geophysical Research, v. 108, 2423, doi:10.1029/2002JB001876.

Gehrels, G.E., et al., 2011, Detrital zircon geochronology of pre-Tertiary strata in the Tibetan-Himalayan orogen: Tectonics, v. 30, Tc5016, doi:10.1029/2011TC002868.

Gong, J., Zhang, J., and Yu, S., 2013, Redefinition of the "Longshoushan Group" outcropped in the eastern segment of Longshoushan on the southern margin of Alxa Block: Evidence from detrital zircon U-Pb dating results: Acta Petrologica et Mineralogica, v. 32, p. 1–22 (in Chinese with English abstract).

Graham, S.A., Hendrix, M.S., Wang, L.B., and Carroll, A.R., 1993, Collisional successor basins of western China: Impact of tectonic inheritance on sand composition: Geological Society of America Bulletin, v. 105, p. 323–344, doi:10.1130/0016-7606(1993)105<0323:CSBOWC>2.3.CO;2.

Guo, J.J., and Zhao, F.Q., 2000, New chronological evidence of the age of Huangyuan in the eastern segment of mid-Qilian massif and its geological significance: Regional Geology of China, v. 19, p. 26–31 (in Chinese with English abstract).

Guo, J.J., Zhao, F.Q., and Li, H.K., 1999, Jinningian collisional granite belt in the eastern sector of the Central Qilian Massif and its implication: Diqiu Xuebao, v. 20, p. 10–15 (in Chinese with English abstract).

Guo, K.Y., Zhang, C.L., Shen, J.L., Ye, H., Wang, A.G., and Li, C., 2004, Chemistry of Statherian volcanic rocks in the western Kunlun Mountains: Geological Bulletin of China, v. 23, p. 130–135 (in Chinese).

Guo, Z.J., Yin, A., Robinson, A., and Jia, C.Z., 2005, Geochronology and geochemistry of deep-drill-core samples from basement of the central Tarim basin: Journal of Asian Earth Sciences, v. 25, p. 45–56, doi:10.1016/j.jseaes.2004.01.016.

Hacker, B.R., Ratschbacher, L., and Liou, J.G., 2004, Subduction, collision, and exhumation in the ultrahigh-pressure Qinling-Dabie orogen, *in* Malpas, J., et al., eds., Aspects of the tectonic evolution of China: Geological Society of London Special Publication 226, p. 157–175, doi:10.1144/GSL.SP.2004.226.01.09.

Hacker, B.R., Wallis, S.R., Ratschbacher, L., Grove, M., and Gehrels, G., 2006, High temperature geochronology constraints on the tectonic history and architecture of the ultrahigh-pressure Dabie-Sulu orogen: Tectonics, v. 25, TC5006, doi:10.1029/2005TC001937.

Harley, S.L., Kelly, N.M., and Möller, A., 2007, Zircon behaviour and the thermal histories of mountain chains: Elements, v. 3, p. 25–30, doi:10.2113/gselements.3.1.25.

He, J., Zhu, W., Ge, R., Zheng, B., and Wu, H., 2014, Detrital zircon U-Pb ages and Hf isotopes of Neoproterozoic strata in the Aksu area, northwestern Tarim Craton: Implications for supercontinent reconstruction and crustal evolution: Precambrian Research, v. 254, p. 194–209, doi:10.1016/j.precamres.2014.08.016.

He, S., Wang, H., Chen, J., Xu, X., Zhang, H., Ren, G., and Yu, J., 2007, LA-ICP-MS U-Pb zircon geochronology of basic dikes within Maxianshan rock group in the central Qilian orogenic belt and its tectonic implications: Journal of China University of Geosciences, v. 18, p. 19–29, doi:10.1016/S1002-0705(07)60015-6.

He, Z.Y., Zhang, Z.M., Zong, K.Q., Wang, W., and Santosh, M., 2012, Neoproterozoic granulites from the northeastern margin of the Tarim Craton: Petrology, zircon U-Pb ages and implications for the Rodinia assembly: Precambrian Research, v. 212, p. 21–33, doi:10.1016/j.precamres.2012.04.014.

Heubeck, C., 2001, Assembly of central Asia during the middle and late Paleozoic, *in* Hendrix, M.S., and Davis, G.A., eds., Paleozoic and Mesozoic tectonic evolution of Central Asia: From continental assembly to intracontinental deformation: Geological Society of America Memoir 194, p. 1–22, doi:10.1130/0-8137-1194-0.1.

Hou, Q., Zhao, Z., Zhang, H., Zhang, B., and Chen, Y., 2006, Indian Ocean-MORB-type isotopic signature of Yushigou ophiolite in North Qilian Mountains and its implications: Science in China Series D, v. 49, p. 561–572, doi:10.1007/s11430-006-0561-8.

Hu, N.G., Xu, A.D., and Yang, J.X., 2005, Characteristics and tectonic environment of Zhigoumen pluton in Longshoushan area: Journal of Earth Sciences and Environment, v. 27, p. 5–11 (in Chinese with English abstract).

Huang, H., Niu, Y.L., Nowell, G., Zhao, Z.D., Yu, X.H., and Mo, X.X., 2015, The nature and history of the Qilian Block in the context of the development of the Greater Tibetan Plateau: Gondwana Research, v. 28, p. 209–224, doi:10.1016/j.gr.2014.02.010.

Huang, J.Q., 1977, The basic outline of China tectonics: Acta Geologica Sinica, v. 52, p. 117–135.

Jiang, C.F., Yang, J.S., Feng, B.G., Zhu, Z.Z., Zhao, M., Chai, Y.C., Shi, X.D., Wang, H.D., and Ha, J.Q., 1992, Opening-closing tectonics of Kunlun Mountains: Beijing, Geological Publishing House, 224 p. (in Chinese with English abstract).

Kröner, A., Wilde, S., O'Brien, P.J., and Li, J.H., 2001, The Hengshan and Wutai complexes of northern China: Lower and upper crustal domains of a late Archean to Paleoproterozoic magmatic arc and significance for the evolution of the North China Craton, *in* Cassidy, K.F., et al., eds., Fourth International Archean Symposium, Perth, Australia, Extended Abstracts: Australian Geological Survey Organisation Geoscience Record, p. 327.

Kröner, A., Wilde, S.A., Li, J.H., and Wang, K.Y., 2005, Age and evolution of a late Archean to Paleoproterozoic upper to lower crustal section in the Wutaishan/Hengshan/Fuping terrain of northern China: Journal of Asian Earth Sciences, v. 24, p. 577–595, doi:10.1016/j.jseaes.2004.01.001.

Kröner, A., Wilde, S.A., Zhao, G.C., O'Brien, P.J., Sun, M., Liu, D.Y., Wan, Y.S., Liu, S.W., and Guo, J.H., 2006, Zircon geochronology and metamorphic evolution of mafic dykes in the Hengshan Complex of northern China: Evidence for late Palaeoproterozoic extension and subsequent high-pressure metamorphism in the North China Craton: Precambrian Research, v. 146, p. 45–67, doi:10.1016/j.precamres.2006.01.008.

Kröner, A., Wilde, S.A., O'Brien, P.J., Li, J.H., Passchier, C.W., Walte, N.P., and Liu, D.Y., 2013a, Field relationships, geochemistry, zircon ages and evolution of a late Archaean to Palaeoproterozoic lower crustal section in the Hengshan terrain of northern China: Acta Geologica Sinica, v. 79, p. 605–629.

Kröner, A., et al., 2013b, Mesoproterozoic (Grenville-age) terranes in the Kyrgyz North Tianshan: Zircon ages and Nd-Hf isotopic constraints on the origin and evolution of basement blocks in the southern Central Asian orogen: Gondwana Research, v. 23, p. 272–295, doi:10.1016/j.gr.2012.05.004.

Kusky, T.M., and Li, J., 2003, Paleoproterozoic tectonic evolution of the North China Craton: Journal of Asian Earth Sciences, v. 22, p. 383–397, doi:10.1016/S1367-9120(03)00071-3.

Kusky, T.M., and Santosh, M., 2009, The Columbia connection in north China, *in* Reddy, S.M., et al., eds., Paleoproterozoic supercontinents and global evolution: Geological Society of London Special Publication 323, p. 49–71, doi:10.1144/SP323.3.

Kusky, T.M., Li, J.H., and Santosh, M., 2007, The Paleoproterozoic North Hebei orogen: North China craton's collisional suture with the Columbia supercontinent: Gondwana Research, v. 12, p. 4–28, doi:10.1016/j.gr.2006.11.012.

Kusky, T.M., et al., 2016, Insights into the tectonic evolution of the North China craton through comparative tectonic analysis: A record of outward growth of Precambrian continents: Earth-Science Reviews, v. 162, p. 387–432, doi:10.1016/j.earscirev.2016.09.002.

Lease, R.O., Burbank, D.W., Zhang, H., Liu, J., and Yuan, D., 2012, Cenozoic shortening budget for the northeastern edge of the Tibetan Plateau: Is lower crustal flow necessary?: Tectonics, v. 31, TC3011, doi:10.1029/2011TC003066.

Li, J., and Kusky, T., 2007, A late Archean foreland fold and thrust belt in the North China Craton: Implications for early collisional tectonics: Gondwana Research, v. 12, p. 47–66, doi:10.1016/j.gr.2006.10.020.

Li, J.H., Kroner, A., Qian, X.L., and O'Brien, P., 2000a, Tectonic evolution of an early Precambrian high-pressure granulite belt in the north China craton: Acta Geologica Sinica, v. 74, p. 246–258.

Li, J.H., Qian, X.L., Huang, X.N., and Liu, S.W., 2000b, Tectonic framework of North China block and its cratonization in the early Precambrian: Yanshi Xuebao, v. 16, p. 1–10.

Li, W.Y., 1991, Sinian tectonic evolution in Longshou Shan region: Northwest Geology, v. 12, no. 2, p. 1–4.

Li, X.H., Li, W.X., Li, Z.X., and Liu, Y., 2008, 850–790 Ma bimodal volcanic and intrusive rocks in northern Zhejiang, South China: A major episode of continental rift magmatism during the breakup of Rodinia: Lithos, v. 102, p. 341–357, doi:10.1016/j.lithos.2007.04.007.

Li, Z.X., Zhang, L., and Powell, C.M., 1995, South China in Rodinia: Part of the missing link between Australia–East Antarctica and Laurentia?: Geology, v. 23, p. 407–410, doi:10.1130/0091-7613(1995)023<0407:SCIRPO>2.3.CO;2.

Li, Z.X., Li, X.H., Zhou, H., and Kinny, P.D., 2002, Grenvillian continental collision in South China: New SHRIMP U-Pb zircon results and implications for the configuration of Rodinia: Geology, v. 30, p. 163–166, doi:10.1130/0091-7613(2002)030<0163:GCCISC>2.0.CO;2.

Li, Z.X., et al., 2008, Assembly, configuration, and break-up history of Rodinia: A synthesis: Precambrian Research, v. 160, p. 179–210, doi:10.1016/j.precamres.2007.04.021.

Lin, Y.H., Zhang, L.F., Ji, J.Q., and Song, S.G., 2010, $^{40}Ar/^{39}Ar$ age of Jiugequan lawsonite blueschists in northern Qilian Mountains and its petrologic significance: Chinese Science Bulletin, v. 55, p. 2021–2027, doi:10.1007/s11434-010-3239-8.

Liou, J.G., Zhang, R.Y., Ernst, W.G., Rumble, D., and Maruyama, S., 1998, High-pressure minerals from deeply subducted metamorphic rocks: Reviews in Mineralogy and Geochemistry, v. 37, p. 33–96.

Liou, J.G., Ernst, W.G., Zhang, R.Y., Tsujimori, T., and Jahn, B.M., 2009, Ultrahigh-pressure minerals and metamorphic terranes: The view from China: Journal of Asian Earth Sciences, v. 35, p. 199–231, doi:10.1016/j.jseaes.2008.10.012.

Liu, Y.J., Neubauer, F., Genser, J., Takasu, A., Ge, X.-H., and Handler, R., 2006, $^{40}Ar/^{39}Ar$ ages of blueschist facies politic schists from Qingshuigou in the Northern Qilian Mountains, western China: The Island Arc, v. 15, p. 187–198, doi:10.1111/j.1440-1738.2006.00508.x.

Lu, S.N., 2002. The Precambrian Geology of Northern Tibet: Geological Publishing.

Lu, S.N., Yu, H.F., and Li, H.K., 2006, Research on Precambrian major problems in China: Beijing, Geological Publishing Press, 206 p. (in Chinese).

Lu, S.N., Li, H.K., Zhang, C.L., and Niu, G.H., 2008, Geological and geochronological evidence for the Precambrian evolution of the Tarim Craton and surrounding continental fragments: Precambrian Research, v. 160, p. 94–107, doi:10.1016/j.precamres.2007.04.025.

Lu, S.N., Li, H.K., Wang, H.C., Chen, Z.H., Zheng, J.K., and Xiang, Z.Q., 2009, Detrital zircon population of Proterozoic metasedimentary strata in the Qinling-Qilian-Kunlun orogen: Yanshi Xuebao, v. 25, p. 2195–2208 (Chinese with English abstract).

Ludwig, K.R., 2003, User's manual for Isoplot 3.00: A geochronological toolkit for Microsoft Excel: Berkeley Geochronology Center Special Publication 4, 70 p.

Ma, X., Shu, L., Santosh, M., and Li, J., 2012, Detrital zircon U-Pb geochronology and Hf isotope data from Central Tianshan suggesting a link with the Tarim Block: Implications on Proterozoic supercontinent history: Precambrian Research, v. 206, p. 1–16, doi:10.1016/j.precamres.2012.02.015.

Maniar, P.D., and Piccoli, P.M., 1989, Tectonic discrimination of granitoids: Geological Society of America Bulletin, v. 101, p. 635–643, doi:10.1130/0016-7606(1989)101<0635:TDOG>2.3.CO;2.

Mattinson, C.G., Menold, C.A., Zhang, J.X., and Bird, D.K., 2007, High- and ultrahigh-pressure metamorphism in the North Qaidam and South Altyn terranes, western China: International Geology Review, v. 49, p. 969–995, doi:10.2747/0020-6814.49.11.969.

Mei, H., Yu, H., Lu, S., and Li, H., 1998, The Archaean tonalite in Dunhuang, Gansu Province: Single-zircon U-Pb age and Nd isotope: Advances in Precambrian Research, v. 21, p. 41–45 (in Chinese with English abstract).

Meng, Q.R., and Zhang, G.W., 1999, Timing of collision of the North and South China blocks: Controversy and reconciliation: Geology, v. 27, p. 123–126.

Menold, C.A., Manning, C.E., Yin, A., Tropper, P., Chen, X.H., and Wang, X.F., 2009, Metamorphic evolution, mineral chemistry and thermobarometry of orthogneiss hosting ultrahigh-pressure eclogites in the North Qaidam metamorphic belt, western China: Journal of Asian Earth Sciences, v. 35, p. 273–284, doi:10.1016/j.jseaes.2008.12.008.

Menold, C.A., Grove, M., Sievers, N., Manning, C.E., Yin, A., Young, E.D., and Ziegler, K., 2016, Argon, oxygen, and boron isotopic evidence documenting ^{40}ArE accumulation in phengite during water-rich high-pressure subduction metasomatism of continental crust: Earth and Planetary Science Letters, v. 446, p. 56–67, doi:10.1016/j.epsl.2016.04.010.

Metcalfe, I., 2011, Tectonic framework and Phanerozoic evolution of Sundaland: Gondwana Research, v. 19, p. 3–21, doi:10.1016/j.gr.2010.02.016.

Middlemost, E.A.K., 1994, Naming materials in the magma/igneous rock system: Earth-Science Reviews, v. 37, p. 215–224, doi:10.1016/0012-8252(94)90029-9.

Nakajima, T., Maruyama, S., Uchiumi, S., Liou, J.G., Wang, X., Xiao, X., and Graham, S.A., 1990, Evidence for late Proterozoic subduction from 700-Myr-old blueschists in China: Nature, v. 346, no. 6281, p. 263–265, doi:10.1038/346263a0.

Pan, G.T., Ding, J., Yao, D., and Wang, L., 2004, Geological map of Qinghai-Xiang (Tibet) plateau and adjacent areas: Chengdu Institute of Geology and Mineral Resources, China Geological Survey, Chengdu Cartographic Publishing House, scale 1:1,500,000.

Pearce, J.A., 1996, Sources and settings of granitic rocks: Episodes, v. 19, p. 120–125.

Pearce, J.A., Harris, N.B.W., and Tindle, A.G., 1984, Trace element discrimination diagrams for the tectonic interpretation of granitic rocks: Journal of Petrology, v. 25, p. 956–983, doi:10.1093/petrology/25.4.956.

Peng, P., Bleeker, W., Ernst, R.E., Söderlund, U., and McNicoll, V., 2011a, U-Pb baddeleyite ages, distribution and geochemistry of 925 Ma mafic dykes and 900 Ma sills in the North China Craton: Evidence for a Neoproterozoic mantle plume: Lithos, v. 127, p. 210–221, doi:10.1016/j.lithos.2011.08.018.

Peng, P., Zhai, M.G., Li, Q., Wu, F., Hou, Q., Li, Z., Li, T., and Zhang, Y., 2011b, Neoproterozoic (900 Ma) Sariwon sills in North Korea: Geochronology, geochemistry and implications for the evolution of the southeastern margin of the North China Craton: Gondwana Research, v. 20, p. 243–254, doi:10.1016/j.gr.2010.12.011.

Polat, A., Kusky, T., Li, J., Fryer, B., Kerrich, R., and Patrick, K., 2005, Geochemistry of Neoarchean (ca. 2.55–2.50 Ga) volcanic and ophiolitic rocks in the Wutaishan greenstone belt, central orogenic belt, North China craton: Implications for geodynamic setting and continental growth: Geological Society of America Bulletin, v. 117, p. 1387–1399, doi:10.1130/B25724.1.

Pullen, A., Kapp, P., Gehrels, G.E., Vervoort, J.D., and Ding, L., 2008, Triassic continental subduction in central Tibet and Mediterranean-style closure of the Paleo-Tethys Ocean: Geology, v. 36, p. 351–354, doi:10.1130/G24435A.1.

Qi, X.X., 2003, Large size ductile strike-slip shearing and the formation of Qilian Caledonian Orogen [Ph.D. thesis]: Beijing, Chinese Academy of Geological Sciences, 119 p.

Qian, Q., Wang, Y.M., Li, H.M., Jia, X.Q., Han, S., and Zhang, Q., 1998, Geochemical characteristics and genesis of diorites from Laohushan, Gansu Province: Acta Petrolei Sinica, v. 14, p. 520–528 (in Chinese with English abstract).

Qinghai Bureau of Geology and Mineral Resources, 1991, Regional geology of Qinghai Province: Beijing, Geological Publishing House, 662 p. (in Chinese with English abstract).

Ratschbacher, L., Hacker, B.R., Calvert, A., Webb, L.E., Grimmer, J.C., McWilliams, M.O., Dong, S.W., and Hu, J., 2003, Tectonics of the Qinling (central China): Tectonostratigraphy, geochronology, and deformation history: Tectonophysics, v. 366, p. 1–53, doi:10.1016/S0040-1951(03)00053-2.

Reith, R.C., 2013, Structural geology of a central segment of the Qilian Shan–Nan Shan thrust belt: Implications for the magnitude of Cenozoic shortening in the northeastern Tibetan Plateau [M.S. thesis]: Los Angeles, University of California, 73 p.

Rojas-Agramonte, Y., Kröner, A., Demoux, A., Xia, X., Wang, W., Donskaya, T., Liu, D., and Sun, M., 2011, Detrital and xenocrystic zircon ages from Neoproterozoic to Palaeozoic arc terranes of Mongolia: Significance for the origin of crustal fragments in the Central Asian orogenic belt: Gondwana Research, v. 19, p. 751–763, doi:10.1016/j.gr.2010.10.004.

Rollinson, H.R., 2014, Using geochemical data: Evaluation, presentation, interpretation: Abingdon, U.K., Routledge, 352 p.

Ryan, W.B., et al., 2009, Global multi-resolution topography synthesis: Geochemistry, Geophysics, Geosystems, v. 10, Q03014, doi:10.1029/2008GC002332.

Santosh, M., Sajeev, K., and Li, J.H., 2006, Extreme crustal metamorphism during Columbia supercontinent assembly: Evidence from North China Craton: Gondwana Research, v. 10, p. 256–266, doi:10.1016/j.gr.2006.06.005.

Santosh, M., Wilde, S.A., and Li, J.H., 2007, Timing of Paleoproterozoic ultrahigh-temperature metamorphism in the North China Craton: Evidence from SHRIMP U-Pb zircon geochronology: Precambrian Research, v. 159, p. 178–196, doi:10.1016/j.precamres.2007.06.006.

Şengör, A.M.C., and Natal'in, B.A., 1996, Paleotectonics of Asia: Fragments of a synthesis, *in* Yin, A., and Harrison, T.M., eds., Tectonic evolution of Asia: New York, Cambridge University Press, p. 486–640.

Shi, R.D., Yang, J.S., and Wu, C.L., 2004, First SHRIMP dating for the formation of the late Sinian Yushigou Ophiolite North Qilian Mountains: Acta Geologica Sinica, v. 78, p. 649–657 (in Chinese with English abstract).

Shu, L.S., and Charvet, J., 1996, Kinematics and geochronology of the Proterozoic Dongxiang-Shexian ductile shear zone: With HP metamorphism and ophiolitic mélange (Jiangnan region, south China): Tectonophysics, v. 267, p. 291–302, doi:10.1016/S0040-1951(96)00104-7.

Shu, L.S., Shi, Y.S., Gou, L.Z., Charvet, J., and Sun, Y., eds., 1995, Plate tectonic evolution and the kinematics of collisional orogeny in the Middle Jiangnan, eastern China: Nanjing University Publication, 174 p. (in Chinese with English Abstract).

Shu, L.S., Deng, X.L., Zhu, W.B., Ma, D.S., and Xiao, W.J., 2011, Precambrian tectonic evolution of the Tarim Block, NW China: New geochronological insights from the Quruqtagh domain: Journal of Asian Earth Sciences, v. 42, p. 774–790, doi:10.1016/j.jseaes.2010.08.018.

Smith, A.D., 2006, The geochemistry and age of ophiolitic strata of the Xinglongshan Group: Implications for the amalgamation of the Central Qilian belt: Journal of Asian Earth Sciences, v. 28, p. 133–142, doi:10.1016/j.jseaes.2005.09.014.

Sobel, E.R., and Arnaud, N., 1999, A possible middle Paleozoic suture in the Altyn Tagh, NW China: Tectonics, v. 18, p. 64–74, doi:10.1029/1998TC900023.

Song, S.G., and Su, L., 1998, Rheological properties of mantle peridotites at Yushigou in the North Qilian Mountains and their implications for plate dynamics: Acta Geologica Sinica, v. 72, p. 131–141, doi:10.1111/j.1755-6724.1998.tb00389.x.

Song, S.G., Zhang, L.F., Niu, Y.L., Su, L., Song, B., and Liu, D.Y., 2006, Evolution from oceanic subduction to continental collision: A case study of the Northern Tibetan Plateau inferred from geochemical and geochronological data: Journal of Petrology, v. 47, p. 435–455, doi: 10.1093/petrology/egi080.

Song, S.G., Su, L., Li, X.H., Zhang, G., Niu, Y.L., and Zhang, L., 2010, Tracing the 850-Ma continental flood basalts from a piece of subducted continental crust in the North Qaidam UHPM belt, NW China: Precambrian Research, v. 183, p. 805–816, doi:1016/j.precamres.2010.09.008.

Song, S.G., Su, L., Li, X.H., Niu, Y.L., and Zhang, L.F., 2012, Grenville-age orogenesis in the Qaidam–Qilian block: The link between South China and Tarim: Precambrian Research, v. 220, p. 9–22, doi:10.1016/j.precamres.2012.07.007.

Song, S.G., Niu, Y.L., Su, L., and Xia, X., 2013, Tectonics of the North Qilian orogen, NW China: Gondwana Research, v. 23, p. 1378–1401, doi:10.1016/j.gr.2012.02.004.

Song, S.G., Niu, Y.L., Su, L., Zhang, C., and Zhang, L., 2014, Continental orogenesis from ocean subduction, continent collision/subduction, to orogen collapse, and orogen recycling: The example of the North Qaidam UHPM belt, NW China: Earth-Science Reviews, v. 129, p. 59–84, doi:10.1016/j.earscirev.2013.11.010.

Song, Z.J., Zhang, H.Y., Hou, D., Liu, C.F., and Liu, W.C., 2017, Discovery and its geological significance of retrograded eclogites in the northern margin of the central Qilian block: Earth Science Frontiers (in press) (in Chinese with English abstract).

Stampfli, G.M., and Borel, G.D., 2002, A plate tectonic model for the Paleozoic and Mesozoic constrained by dynamic plate boundaries and restored synthetic oceanic isochrones: Earth and Planetary Science Letters, v. 196, p. 17–33, doi:10.1016/S0012-821X(01)00588-X.

Sun, J.F., Yang, J.H., Wu, F.Y., and Wilde, S.A., 2012, Precambrian crustal evolution of the eastern North China Craton as revealed by U-Pb ages and Hf isotopes of detrital zircons from the Proterozoic Jing' eryu Formation: Precambrian Research, v. 200, p. 184–208, doi:10 .1016/j.precamres.2012.01.018.

Sun, S.S., and McDonough, W.F., 1989, Chemical and isotopic systematics of oceanic basalts: Implications for mantle composition and processes, *in* Saunders, A.D., and Norry, M.J., eds., Magmatism in the ocean basins: Geological Society of London Special Publication 42, p. 313–345, doi:10.1144/GSL.SP.1989.042.01.19.

Taylor, M., and Yin, A., 2009, Active structures of the Himalayan-Tibetan orogen and their relationships to earthquake distribution, contemporary strain field, and Cenozoic volcanism: Geosphere, v. 5, p. 199–214, doi:10.1130/GES00217.1.

Trap, P., Faure, M., Lin, W., and Monié, P., 2007, Late Paleoproterozoic (1900–1800 Ma) nappe-stacking and polyphase deformation in the Hengshan–Wutaishan area: Implications for the understanding of the Trans-North-China Belt, North China Craton: Precambrian Research, v. 156, p. 85–106, doi:10.1016/j.precamres.2007.03.001.

Trap, P., Faure, M., Lin, W., Bruguier, O., and Monié, P., 2008, Contrasted tectonic styles for the Paleoproterozoic evolution of the North China Craton. Evidence for a ~2.1 Ga thermal and tectonic event in the Fuping Massif: Journal of Structural Geology, v. 30, p. 1109–1125, doi:10.1016/j.jsg.2008.05.001.

Trap, P., Faure, M., Lin, W., Le Breton, N., and Monié, P., 2011, Paleoproterozoic tectonic evolution of the trans-North China orogen: Toward a comprehensive model: Precambrian Research, v. 222–223, p. 191–211, doi:10.1016/j.precamres.2011.09.008.

Trap, P., Faure, M., Lin, W., Le Breton, N., and Monié, P., 2012, Paleoproterozoic tectonic evolution of the Trans-North China Orogen: Toward a comprehensive model: Precambrian Research, v. 222–223, p. 191–211, doi:10.1016/j.precamres.2011.09.008.

Tseng, C.Y., Yang, H.Y., Wan, Y., Liu, D., Wen, D.J., Lin, T.C., and Tung, K.A., 2006, Finding of Neoproterozoic (775 Ma) magmatism recorded in metamorphic complexes from the North Qilian orogen: Evidence from SHRIMP zircon U-Pb dating: Chinese Science Bulletin, v. 51, p. 963–970, doi:10.1007/s11434-006-0963-1.

Tseng, C.Y., Yang, H.J., Yang, H.Y., Liu, D.Y., Tsai, C.L., Wu, H.Q., and Zuo, G.C., 2007, The Dongcaohe ophiolite from the North Qilian Mountains: A fossil oceanic crust of the Paleo-Qilian ocean: Chinese Science Bulletin, v. 52, p. 2390–2401, doi:10.1007/s11434-007-0300-3.

Tseng, C.Y., Yang, H.J., Yang, H.Y., Liu, D.Y., Wu, C.L., Cheng, C.K., Chen, C.H., and Ker, C.M., 2009, Continuity of the North Qilian and North Qinling orogenic belts, central orogenic system of China: Evidence from newly discovered Paleozoic adakitic rocks: Gondwana Research, v. 16, p. 285–293, doi:10.1016/j.gr.2009.04.003.

Tung, K., Yang, H.J., Yang, H.Y., Liu, D., Zhang, J., Wan, Y., and Tseng, C.Y., 2007, SHRIMP U-Pb geochronology of the zircons from the Precambrian basement of the Qilian Block and its geological significances: Chinese Science Bulletin, v. 52, p. 2687–2701, doi:10.1007 /s11434-007-0356-0.

Tung, K.A., Yang, H.Y., Liu, D.Y., Zhang, J.X., Yang, H.J., Shau, Y.H., and Tseng, C.Y., 2013, The Neoproterozoic granitoids from the Qilian block, NW China: Evidence for a link between the Qilian and South China blocks: Precambrian Research, v. 235, p. 163–189, doi:10.1016 /j.precamres.2013.06.016.

Turner, S.A., 2010, Sedimentary record of late Neoproterozoic rifting in the NW Tarim Basin, China: Precambrian Research, v. 181, p. 85–96, doi:10.1016/j.precamres.2010.05.015.

Turner, S.P., Foden, J.D., and Morrison, R.S., 1992, Derivation of some A-type magmas by fractionation of basaltic magma—An example from the Padthaway Ridge, South Australia: Lithos, v. 28, p. 151–179, doi:10.1016/0024-4937(92)90029-X.

Vincent, S.J., and Allen, M.B., 1999, Evolution of the Minle and Chaoshui Basins, China: Implications for Mesozoic strike-slip basin formation in Central Asia: Geological Society of America Bulletin, v. 111, p. 725–742.

Wan, Y.S., Xu, Z.Q., and Yang, J.S., 2001, Ages and compositions of the Precambrian high grade basement of the Qilian terrane and its adjacent areas: Acta Geologica Sinica, v. 75, p. 375–384, doi:10.1111/j.1755-6724.2001.tb00055.x.

Wan, Y.S., Liu, D.Y., Wang, W., Song, T., Kröner, A., Dong, C.Y., Zhou, H.Y., and Yin, X., 2011, Provenance of Meso- to Neoproterozoic cover sediments at the Ming Tombs, Beijing, North China Craton: An integrated study of U-Pb dating and Hf isotopic measurement of detrital zircons and whole-rock geochemistry: Gondwana Research, v. 20, p. 219–242, doi:10.1016/j.gr.2011.02.009.

Wan, Y.S., Liu, D.Y., Wang, S.J., Yang, E.X., Wang, W., Dong, C.Y., Zhou, H.Y., Du, L.L., Yang, Y.H., and Diwu, C.R., 2013, Is the Ordos block Archean or Paleoproterozoic in age? Implications for the Precambrian evolution of the North China Craton: American Journal of Science, v. 313, p. 683–711, doi:10.2475/07.2013.03.

Wan, Y.S., Liu, D.Y., Dong, C.Y., Xie, H.Q., Kröner R. A., Ma, M.Z., Liu, S.J., Xie, S.W., and Ren, P., 2015, Formation and evolution of Archean continental crust of the North China Craton: Precambrian geology of China: Berlin, Heidelberg, Springer, p. 59–136.

Wang, A.G., Zhang, C.L., and Guo, K.Y., 2004, Depositional types and its tectonic significance of lower member of Nanhuan System in north margin of West Kunlun: Journal of Stratigraphy, v. 28, p. 248–256 (in Chinese with English abstract).

Wang, C., et al., 2015a, Recognition and tectonic implications of an extensive Neoproterozoic volcano-sedimentary rift basin along the southwestern margin of the Tarim Craton, northwestern China: Precambrian Research, v. 257, p. 65–82, doi:10.1016/j.precamres.2014.11.022.

Wang, C., Zhang, J.H., Li, M., Li, R.S., and Peng, Y., 2015b, Generation of ca. 900–870 Ma bimodal rifting volcanism along the southwestern margin of the Tarim Craton and its implications for the Tarim–North China connection in the early Neoproterozoic: Journal of Asian Earth Sciences, v. 113, p. 610–625, doi:10.1016/j.jseaes.2015.08.002.

Wang, H.Z., and Mo, X.X., 1995, An outline of the tectonic evolution of China: Episodes, v. 18, p. 6–16.

Wang, L.J., Griffin, W.L., Yu, J.H., and O'Reilly, S.Y., 2012, Early crustal evolution in the western Yangtze Block: Evidence from U-Pb and Lu-Hf isotopes on detrital zircons from sedimentary rocks: Precambrian Research, v. 222, p. 368–385, doi:10.1016/j.precamres.2011.08.001.

Wang, Q., and Liu, X.Y., 1976, The ancient oceanic crust and its tectonic implications, North Qilian Mountains, China: Scienta Geologica Sinica, no. 1, p. 42–55 (in Chinese with English abstract).

Wang, S.J., Li, S.G., Chen, L.J., He, Y.S., An, S.C., and Shen, J., 2013a, Geochronology and geochemistry of leucosomes in the North Dabie terrane, East China: Implication for post UHPM crustal melting during exhumation: Contributions to Mineralogy and Petrology, v. 165, p. 1009–1029, doi:10.1007/s00410-012-0845-2.

Wang, Y., Fan, W., Zhang, G., and Zhang, Y., 2013b, Phanerozoic tectonics of the South China block: Key observations and controversies: Gondwana Research, v. 23, p. 1273–1305, doi:10.1016/j.gr.2012.02.019.

Whalen, J.B., Currie, K.L., and Chappell, B.W., 1987, A-type granites: Geochemical characteristics, discrimination and petrogenesis: Contributions to Mineralogy and Petrology, v. 95, p. 407–419, doi:10.1007/BF00402202.

Wu, C., Yin, A., Zuza, A.V., Zhang, J., Liu, W., and Ding, L., 2016, Pre-Cenozoic geologic history of the central and northern Tibetan Plateau and the role of Wilson cycles in constructing the Tethyan orogenic system: Lithosphere, v. 8, p. 254–292, doi:10.1130/L494.1.

Wu, C.L., Yang, J.S., Yang, H.Y., Wooden, J.L., Shi, R.D., Chen, S.Y., and Zheng, Q.G., 2004, Two types of I-type granite dating and geological significance from North Qilian, NW China: Yanshi Xuebao, v. 20, p. 425–432 (in Chinese with English abstract).

Wu, C.L., Yao, S.Z., Yang, J.S., Zeng, L.S., Chen, S.Y., Li, H.B. Qi, X.X., Wooden, J.L., and Mazdab, F.K., 2006, The granite evidence of the early Paleozoic two-way subduction in the North Qilian Mountains: Geology in China, v. 33, p. 1197–1208 (in Chinese with English abstract).

Wu, C.L., Xu, X.Y., Gao, Q.M., Li, X.M., Lei, M., Gao, Y.H., Frost, R.B., and Wooden, J.L., 2010, Early Palaeozoic granitoid magmatism and tectonic evolution in North Qilian, NW China: Yanshi Xuebao, v. 26, p. 1027–1044 (in Chinese with English abstract).

Wu, L., 2013, The detrital-zircon U-Pb dating and provenance analysis for the Triassic sandstone in Qilian Shan, northeastern margin of the Tibetan Plateau [M.S. thesis]: Beijing, China University of Geosciences, 72 p.

Xia, X.H., and Song, S.G., 2010, Forming age and tectono-petrogeneses of the Jiugequan ophiolite in the North Qilian Mountain, NW China: Chinese Science Bulletin, v. 55, p. 1899–1907, doi:10.1007/s11434-010-3207-3.

Xia, X.H., Song, S.G., and Niu, Y.L., 2012, Tholeiite–boninite terrane in the North Qilian suture zone: Implications for subduction initiation and back-arc basin development: Chemical Geology, v. 328, p. 259–277, doi:10.1016/j.chemgeo.2011.12.001.

Xiang, Z.Q., Lu, S.N., Li, H.K., Li, H.M., Song, B., and Zheng, J.K., 2007, SHRIMP U-Pb zircon age of gabbro in Aoyougou in the western segment of the North Qilian Mountains, China and its geological implications: Geological Bulletin of China, v. 26, p. 1686–1691.

Xiao, L.L., Wu, C.M., Zhao, G.C., Guo, J.H., and Ren, L.D., 2011, Metamorphic P-T paths of the Zanhuang amphibolites and metapelites: Constraints on the tectonic evolution of the Paleoproterozoic Trans-North China orogen: International Journal of Earth Sciences, v. 100, p. 717–739, doi:10.1007/s00531-010-0522-5.

Xiao, W.J., Windley, B.F., Hao, J., and Zhai, M., 2003, Accretion leading to collision and the Permian Solonker suture, Inner Mongolia, China: Termination of the central Asian orogenic belt: Tectonics, v. 22, 1069, doi:10.1029/2002TC001484.

Xiao, W.J., Windley, B.F., Yong, Y., Yan, Z., Yuan, C., Liu, C.Z., and Li, J.L., 2009, Early Paleozoic to Devonian multiple-accretionary model for the Qilian Shan, NW China: Journal of Asian Earth Sciences, v. 35, p. 323–333, doi:10.1016/j.jseaes.2008.10.001.

Xiao, X.C., Chen, G.M., and Zhu, Z.Z., 1978, A preliminary study on the tectonics ancient ophiolites in the Qilian Mountain, northwest China: Acta Geologica Sinica, v. 4, p. 279–295 (in Chinese with English abstract).

Xu, X., Song, S.G., Su, L., Li, Z.X., Niu, Y.L., and Allen, M.B., 2015, The 600–580 Ma continental rift basalts in North Qilian Shan, northwest China: Links between the Qilian-Qaidam block and SE Australia, and the reconstruction of East Gondwana: Precambrian Research, v. 257, p. 47–64, doi:10.1016/j.precamres.2014.11.017.

Xu, Y.J., Cawood, P., Du, Y.S., Zhong, Z.Q., and Hughes, N.C., 2014, Terminal suturing of Gondwana along the southern margin of South China Craton: Evidence from detrital zircon U-Pb ages and Hf isotopes in Cambrian and Ordovician strata, Hainan Island: Tectonics, v. 33, p. 2490–2504, doi:10.1002/2014TC003748.

Xu, Z.Q., He, B.Z., Zhang, C.L., Zhang, J.X., Wang, Z.M., and Cai, Z.H., 2013, Tectonic framework and crustal evolution of the Precambrian basement of the Tarim Block in NW China: New geochronological evidence from deep drilling samples: Precambrian Research, v. 235, p. 150–162, doi:10.1016/j.precamres.2013.06.001.

Xue, N., Wang, J., Tan, S.X., Lin, H., Li, W.F., Ren, J.Q., and Liu, S.J., 2009, Geological significance of granite of Jinningian age in Yeniugou-Tuole region on the northern margin of Central Qilian block [Nature Science]: Journal of Qinghai University, v. 27, p. 23–28.

Yan, Z., Xiao, W.J., Wang, Z., and Li, J., 2007, Integrated analyses constraining the provenance of sandstones, mudstones, and conglomerates, a case study: The Laojunshan conglomerate, Qilian orogen, northwest China: Canadian Journal of Earth Sciences, v. 44, p. 961–986, doi:10.1139/e07-010.

Yang, H., Zhang, H.F., Luo, B.J., Gao, Z., Guo, L., and Xu, W.C., 2016, Generation of peraluminous granitic magma in a post-collisional setting: A case study from the eastern Qilian Orogen, NE Tibetan Plateau: Gondwana Research, v. 36, p. 28–45, doi:10.1016/j.gr.2016.04.006.

Yang, J.S., Xu, Z.Q., Zhang, J.X., Song, S.G., Wu, C.L., Shi, R.D., Li, H.B., and Brunel, M., 2002, Early Palaeozoic north Qaidam UHP metamorphic belt on the north-eastern Tibetan plateau and a paired subduction model: Terra Nova, v. 14, p. 397–404, doi:10.1046/j.1365-3121.2002.00438.x.

Ye, Z., Gao, R., Li, Q., Zhang, H., Shen, X., Liu, X., and Gong, C., 2015, Seismic evidence for the North China plate underthrusting beneath northeastern Tibet and its implications for plateau growth: Earth and Planetary Science Letters, v. 426, p. 109–117, doi:10.1016/j.epsl.2015.06.024.

Yin, A., 2010, Cenozoic tectonic evolution of Asia: A preliminary synthesis: Tectonophysics, v. 488, p. 293–325, doi:10.1016/j.tecto.2009.06.002.

Yin, A., and Harrison, T., 2000, Geologic evolution of the Himalayan-Tibetan orogeny: Annual Review of Earth and Planetary Sciences, v. 28, p. 211–280, doi:10.1146/annurev.earth.28.1.211.

Yin, A., and Nie, S., 1993, An indentation model for the North and South China collision and the development of the Tan-Lu and Honam fault systems, eastern Asia: Tectonics, v. 12, p. 801–813, doi:10.1029/93TC00313.

Yin, A., and Nie, S.Y., 1996, A Phanerozoic palinspastic reconstruction of China and its neighboring regions, *in* Yin, A., and Harrison, T.M., eds., The tectonic evolution of Asia: New York, Cambridge University Press, p. 442–485.

Yin, A., Manning, C.E., Lovera, O., Menold, C.A., Chen, X.H., and Gehrels, G.E., 2007a, Early Paleozoic tectonic and thermomechanical evolution of ultrahigh-pressure (UHP) metamorphic rocks in the northern Tibetan Plateau, northwest China: International Geology Review, v. 49, p. 681–716, doi:10.2747/0020-6814.49.8.681.

Yin, A., Dang, Y.Q., Zhang, M., McRivette, M.W., Burgess, W.P., and Chen, X.H., 2007b, Cenozoic tectonic evolution of Qaidam Basin and its surrounding regions (part 2): Wedge tectonics in southern Qaidam Basin and the Eastern Kunlun Range, *in* Sears, J.W., et al., eds., Whence the mountains? Inquiries into the evolution of orogenic systems: A volume in honor of Raymond A. Price: Geological Society of America Special Paper 433, p. 369–390, doi:10.1130/2007.2433(18).

Yin, A., Dang, Y.Q., Wang, L.C., Jiang, W.M., Zhou, S.P., Chen, X.H., Gehrels, G.E., and McRivette, M.W., 2008, Cenozoic tectonic evolution of Qaidam basin and its surrounding regions (Part 1): The southern Qilian Shan-Nan Shan thrust belt and northern Qaidam basin: Geological Society of America Bulletin, v. 120, p. 813–846, doi:10.1130/B26180.1.

Yu, J.H., Wang, L.J., Griffin, W.L., O'Reilly, S.Y., Zhang, M., Li, C.Z., and Shu, L.S., 2009, A Paleoproterozoic orogeny recorded in a long-lived cratonic remnant (Wuyishan terrane), eastern Cathaysia Block, China: Precambrian Research, v. 174, p. 347–363, doi:10.1016/j.precamres.2009.08.009.

Zhang, C.L., Li, Z.X., Li, X.H., Ye, H., Wang, A., and Guo, K.Y., 2006, Neoproterozoic bimodal intrusive complex in the southwestern Tarim Block, northwest China: Age, geochemistry, and implications for the rifting of Rodinia: International Geology Review, v. 48, p. 112–128, doi:10.2747/0020-6814.48.2.112.

Zhang, J.X., Wan, Y.S., Meng, F.C., Yang, J.S., and Xu, Z.Q., 2003, Geochemistry, Sm-Nd and U-Pb isotope study of gneisses (schists) enclosing eclogites in the North Qaidam Mountains—Deeply subducted Precambrian metamorphic basement: Yanshi Xuebao, v. 19, p. 443–451 (in Chinese with English abstract).

Zhang, J.X., Meng, F.C., and Wan, Y.S., 2007, A cold Early Palaeozoic subduction zone in the North Qilian Mountains, NW China: Petrological and U-Pb geochronological constraints: Journal of Metamorphic Geology, v. 25, p. 285–304, doi:10.1111/j.1525-1314.2006.00689.x.

Zhang, L., Chen, R.X., Zheng, Y.F., Hu, Z., and Xu, L., 2017, Whole-rock and zircon geochemical distinction between oceanic-and continental-type eclogites in the North Qaidam orogen, northern Tibet: Gondwana Research, v. 44, p. 67–88.

Zhang, L.Y., et al., 2014, Age and geochemistry of western Hoh-Xil–Songpan-Ganzi granitoids, northern Tibet: Implications for the Mesozoic closure of the Paleo-Tethys Ocean: Lithos, v. 190, p. 328–348, doi:10.1016/j.lithos.2013.12.019.

Zhang, S.H., Zhao, Y., Yang, Z.Y., He, Z.F., and Wu, H., 2009, The 1.35 Ga diabase sills from the northern North China Craton: Implications for breakup of the Columbia (Nuna) supercontinent: Earth and Planetary Science Letters, v. 288, p. 588–600, doi:10.1016/j.epsl.2009.10.023.

Zhang, S.H., Zhao, Y., and Santosh, M., 2012, Mid-Mesoproterozoic bimodal magmatic rocks in the northern North China Craton: Implications for magmatism related to breakup of the Columbia supercontinent: Precambrian Research, v. 222–223, p. 339–367, doi:10.1016/j.precamres.2011.06.003.

Zhao, G., and Cawood, P., 2012, Precambrian geology of China: Precambrian Research, v. 222–223, p. 13–54, doi:10.1016/j.precamres.2012.09.017.

Zhao, G.C., Wilde, S.A., Cawood, P.A., and Lu, L.Z., 1998, Thermal evolution of Archean basement rocks from the eastern part of the North China Craton and its bearing on tectonic setting: International Geology Review, v. 40, p. 706–721, doi:10.1080/00206819809465233.

Zhao, G.C., Wilde, S.A., Cawood, P.A., and Lu, L.Z., 1999, Tectonothermal history of the basement rocks in the western zone of the North China Craton and its tectonic implications: Tectonophysics, v. 310, p. 37–53, doi:10.1016/S0040-1951(99)00152-3.

Zhao, G., Cawood, P.A., Li, S., Wilde, S.A., Sun, M., Zhang, J., He, Y., and Yin, C., 2012, Amalgamation of the North China Craton: Key issues and discussion: Precambrian Research, v. 222, p. 55–76, doi:10.1016/j.precamres.2012.09.016.

Zhao, Z., Wei, J., Fu, L., Liang, S., and Zhao, S., 2017, The early Paleozoic Xitieshan syn-collisional granite in the North Qaidam ultrahigh-pressure metamorphic belt, NW China: Petrogenesis and implications for continental crust growth: Lithos, v. 278–281, p. 140–152, doi:10.1016/j.lithos.2017.01.019.

Zhou, Z.G., Wang, G.S., Zhang, D., Gu, Y.C., Zhu, W.P., Liu, C.F., Zhao, X.Q., and Hu, M.M., 2016, Zircon ages of gabbros in the Siziwangqi, Inner Mongolia and its constraint on the formation time of the Bayan Obo Group: Yanshi Xuebao, v. 32, p. 1809–1822 (in Chinese with English abstract).

Zhu, W., Zhang, Z., Shu, L., Lu, H., Su, J., and Yang, W., 2008, SHRIMP U-Pb zircon geochronology of Neoproterozoic Korla mafic dykes in the northern Tarim Block, NW China: Implications for the long-lasting breakup process of Rodinia: Journal of the Geological Society [London], v. 165, p. 887–890, doi:10.1144/0016-76492007-174.

Zuo, G.C., and Liu, J.C., 1987, The evolution of tectonic of early Paleozoic tectonic evolution in north Qilian range: China: Chinese Journal of Geology, v. 1, p. 14–24.

Zuza, A.V., 2016, Tectonic evolution of the northeastern Tibetan Plateau [Ph.D thesis]: Los Angeles, University of California, 521 p.

Zuza, A.V., and Yin, A., 2014, Initial and boundary conditions for the evolution of the Central Asian orogenic system (CAOS): The Balkatach hypothesis: Geological Society of America Abstracts with Programs, v. 46, no. 6, p. 789.

Zuza, A.V., and Yin, A., 2016, Continental deformation accommodated by non-rigid passive bookshelf faulting: An example from the Cenozoic tectonic development of northern Tibet: Tectonophysics, v. 677–678, p. 227–240, doi:10.1016/j.tecto.2016.04.007.

Zuza, A.V., Reith, R.C., Yin, A., Dong, S.W., Zhang, Y.X., and Wu, C., 2013, Structural and tectonic framework of the Qilian Shan-Nan Shan thrust belt, northeastern Tibetan Plateau: Acta Geologica Sinica, v. 87, p. 1–111, doi:10.1111/1755-6724.12148_1.

Zuza, A.V., Cheng, X., and Yin, A., 2016, Testing models of Tibetan Plateau formation with Cenozoic shortening estimates across the Qilian Shan–Nan Shan thrust belt: Geosphere, v. 12, p. 501–532, doi:10.1130/GES01254.1.

MANUSCRIPT RECEIVED 22 DECEMBER 2016
REVISED MANUSCRIPT RECEIVED 1 MARCH 2017
MANUSCRIPT ACCEPTED 26 APRIL 2017

Printed in the USA